TÉCNICO LISBOA

Langmuir Monolayers of Perfluorinated Alcohols: A Molecular Dynamics Approach

Duarte Coutinho de Almeida Vila Nova

Thesis to obtain the Master of Science Degree in

Chemical Engineering

Supervisor: Doctor Pedro Morgado

Examination Committee

Chairperson: Professor Doctor Francisco Lemos

Supervisor: Doctor Pedro Morgado

Member of the Committee: Doctor Adilson Alves de Freitas

January 2021

Acknowledgments

Firstly, I would like to thank Professor Eduardo Filipe for bringing me into contact with the chemical computer simulations field for the first time in his fourth year introductory course. It led me to gain such an interest and insight that ultimately steered me to apply for this particular thesis. I truly appreciate the opportunity given, his guidance and the friendly and supportive work environment that has been created. Also, I am very glad to have had some of the findings of this study presented in a published paper and for being among the members of an incredible research team.

Additionally, I would also like to thank Doctor Pedro Morgado for going well and beyond to provide the most substantiated and complete answers he could for the presented questions. I will not forget his integrity and the constant effort to share his expertise to the very best of his ability. I would also like to acknowledge PhD student Eng. Gonçalo Silva who was instrumental to develop my computational skills and understanding of the used software.

I also have to express my deep gratitude towards PhD student Eng. Pedro Silva, with whom I spent countless hours discussing this work. I greatly admire his work ethic and value his input, which was essential to develop this study and bring it to a close.

Finally, I am truly grateful to my family, whom have supported and enabled me to pursue this long, tough but fruitful path.

Thank you all.

Abstract

The simultaneous hydrophobicity and lipophobicity of fluorinated amphiphiles, as well as their ability to form isolated, condensed and ordered Langmuir films makes them very significant for interface-directed applications.

Recent experimental research has found that perfluorinated alcohols ($C_nF_{2n+1}CH_2OH$) tend to produce highly organized and cohesive domains even at very low surface densities, which was confirmed in this work through Molecular Dynamics simulations. Furthermore, it was showed that the fluorocarbon monolayers structural integrity is reduced as the number of molecules that comprise the aggregate decreases. It was also demonstrated that perfluorinated alcohols form highly ordered domains compared to those of their hydrogenated homologues. These results were fully validated since Grazing Incidence X-Ray Diffraction (GIXD) spectra calculated from the simulated trajectories was found to be in very good agreement with experimental spectra data, where both showed the inherent tendency of the fluorinated amphiphiles to organize in a 2D hexagonal lattice.

Keywords: Perfluorinated alcohols; Langmuir films; Grazing Incidence X-Ray Diffraction; Molecular Dynamics simulations

Resumo

A simultânea hidrofobicidade e lipofobicidade dos compostos anfifílicos fluorados, bem como a sua capacidade para formar filmes de Langmuir isolados, condensados e ordenados tornam-nos muito importantes para aplicações de interface.

Estudos experimentais recentes demonstraram que álcoois perfluorados ($C_nF_{2n+1}CH_2OH$) tendem a formar agregados coesos e muito bem organizados, o que foi confirmado neste trabalho através de simulações de Dinâmica Molecular. Adicionalmente, foi demonstrado que a integridade estrutural das monocamadas dos fluorocarbonos é reduzida à medida que o número de moléculas que formam os agregados é diminuído. Foi também comprovado que os álcoois perfluorados formam domínios muito bem ordenados comparados com os dos compostos hidrogenados equivalentes. Estes resultados foram validados, uma vez que os espectros de Difração de Raios-X Rasantes calculados a partir das trajectórias simuladas estavam em muito boa conformidade com os dados dos espectros experimentais, em que ambos indicaram a tendência dos compostos anfifílicos fluorados em se organizarem numa estrutura hexagonal 2D.

Palavras-Chave: Álcoois perfluorados; Filmes de Langmuir; Difração de Raios-X Rasantes; Simulações de Dinâmica Molecular

Contents

List of Tables

List of Figures

List of Acronyms

F18OH	1H,1H-Perfluoro-1-octadecanol.
H18OH	1-Octadecanol.
MD	Molecular Dynamics.
2D	Two Dimensional.
GIXD	Grazing Incidence X-Ray Diffraction.
AFM	Atomic Force Microscopy.
G	Gas phase.
LE	Liquid Expanded phase.
C	Condensed phase.
PBC	Periodic Boundary Conditions.
OPLS-AA	Optimized Potentials for Liquid Simulations - All Atoms.
RB	Ryckaert-Bellemans.
LJ	Lennard-Jones.
VMD	Visual Molecular Dynamics.
LINCS	Linear Constraint Solver.
PME	Particle Mesh Ewald.
L-OPLS	Optimized OPLS-AA parameter set for long hydrocarbons.
SPC/E	Extended Simple Point Charge Model.
FWHM	Full Width at Half Maximum.
OP	Order Parameter.
F14OH	1H,1H-Perfluoro-1-tetradecanol.
F16OH	1H,1H-Perfluoro-1-hexadecanol.
F12OH	1H,1H-Perfluoro-1-dodecanol.
H16OH	1-hexadecanol.
H14OH	1-tetradecanol.
H12OH	1-dodecanol.

List of Symbols

A – Effective molecular area

C_n - Constants for Ryckaert-Bellemans potential

d_{hk} – Hexagonal lattice parameter

ε_{ij} - Lennard-Jones energy parameter for interaction between atoms i and j

ε_0 - Absolute electric permittivity of vacuum

f_i - Interaction forces of particle i

θ_{ijk} – Bend angle

θ_{eq} – Equilibrium Bend angle

k – Strength parameter

l_c – Coherence length

m – Function order

m_i – Mass of particle i

N - number of alcohol molecules in the simulation box

Q_i – Charge of particle i

Q_{xy} - In-plane peak position for the GIXD spectra

Q_z - Rod profile peak position for the GIXD spectra

$\vec{r}_i$ - molecular vector between the carbon bonded to the alcohol group and the terminal carbon

r_i – Position of particle i

r_{ij} - Inter-atomic distance between atoms i and j

r_{eq} - Equilibrium bond stretch distance

σ_{ij} - Lennard-Jones potential zero-crossing distance between atoms i and j

t – Time

U – Potential energy

$u_{intramolecular}$ – Intramolecular potential energy

$u_{Lennard-Jones}$ – Lennard-Jones potential energy

$u_{Coulomb}$ – Coulomb's Law potential energy

ϕ_{ijkl} – Dihedral angle

1. Introduction

When compared with their hydrogenated equivalents, perfluorinated alcohols have been lacking in research and understanding. Simultaneously, this type of compound has enhanced amphiphilicity and a high degree of lipophobicity and can be used in applications that range from water proof coating to biomedical devices, making it of interest to further study.

Alongside the exponential growth of computing power, molecular dynamics (MD) algorithms and software have improved dramatically over the years [1]. Additionally, with the constant improvement of the available models, simulations can take place in a viable time frame and meaningful scale that accurately reproduce real systems.

The MD simulation method can offer unique molecular insight and framework versatility, which are very useful to understand fluorinated alcohols structure and behavior in a *quasi*-two-dimensional system (Langmuir monolayer) at the air-water interface, the subject of this thesis.

1.1. Compounds Overview

The compounds in this study fall under the groups of 1H,1H-perfluorinated alcohols ($C_nF_{2n+1}CH_2OH$) and hydrogenated alcohols ($C_nH_{2n+1}OH$). Throughout this text, the names will be abbreviated in accordance with the number of carbons in the chain and the nature of the hydrophobic moiety. Example: 1H,1H-perfluoro-1-octadecanol as F18OH or H18OH for the homologue alcohol with a fully hydrogenated chain.

1.2. Fluorinated Compounds

Within the fluorinated compounds in study, the chains are almost entirely fluorinated except for the terminal carbon, which is bonded to the alcohol group and two hydrogen atoms. Due to the high electronegativity of the fluorine atoms, these have a high ionization potential and very low polarizability [2]. Simultaneously, the overlapping of orbitals is very effective and the dense electron cloud of the fluorine atoms results in a repellent sheath that protects the perfluoroalkane chain against the approach of other reactants. This makes the C - F bond the strongest single bond found in organic chemistry and a very stable one, resulting in chemical and biological inertness. The low polarization of fluorine leads to low Van der Waals interactions, generating low surface tensions, high fluidity, high vapor pressure, high compressibility, high gas solubility, high spreading coefficient, extreme lipophobicity, and high hydrophobicity (and consequently low water solubility) [3, 4, 5].

Fluorinated chains' properties and physicochemical behavior strongly contrast with those of their hydrogenated counterpart. Despite both atoms being relatively small, fluorine is significantly larger than hydrogen (Van der Waals radius of 1.47 Å vs. 1.20 Å), which results in bulkier chains with a higher

cross-section (30 $Å^2$ vs 20 $Å^2$) and higher molar volumes [6, 7, 8]. Accordingly, the larger fluorine atoms increase the stiffness of the perfluorinated chains [9, 10], resulting in a higher *gauche*/*trans* energy difference than for hydrogenated ones thus greatly favoring *trans* over *gauche* conformations [11, 12]. The *trans* arrangement also has small deviations that produce a helical structure to minimize steric hindrance [13, 14].

The rare combination of hydrophobicity and lipophobicity promotes separation and compartmentalization at a nanometric scale [15]. With the addition of polar groups, amphiphilic molecules with a surfactant quality can be obtained. In fact, even short chain length molecules such as $C_{10}F_{21}(CH_2)_2OH$ (1,1,2,2-tetrahydrohenicosafluorododecanol) have been found to form highly stable monolayers at the air-water interface [16]. These molecules consist of two distinct parts: a hydrophilic/polar “head” group and a hydrophobic/non-polar “tail” group, where the former functions as an anchor to the water surface, whereas the “tail” is directed to the air, creating an insoluble structure: a Langmuir film.

1.2.1. Applications

Due to their biocompatible and chemically inert nature, fluorocarbons have raised interest in the medical industry. Since they have high gas dissolving capacity, they are used as oxygen carriers and blood substitutes [17]. Moreover, they are also used in molecular imaging, as fluids in eye surgery, and in drug and gene delivery [18, 19, 20, 21, 22]. Beyond the medical field, this type of compound can also be found in solvents for biphasic extraction processes [23], fire extinguishers [24], and lubricants [25]. The surfactant quality of the amphiphilic fluorocarbons is also useful in applications such as the leveling of paints and polishes and the synthesis of liquid crystals [2]. Lastly, the films are also used as templates for nanomaterial fabrication through the Langmuir-Blodgett technique [26].

1.3. Langmuir monolayers

A Langmuir monolayer or Langmuir film is defined as a monomolecular insoluble film on the surface of a liquid and is most frequently composed of pseudo-2D systems of amphiphilic molecules settled on an air-water interface [27].

In these films, the molecules have positional and orientational freedom, which can obviously be affected by other variables such as temperature, pH, compression, and the presence of ions. Despite the more recent development of microscopic techniques such as Grazing Incidence X-Ray Diffraction (GIXD) and Atomic Force Microscopy (AFM), surface pressure-area isotherms (or Langmuir isotherms) were the primary source of thermodynamical data for Langmuir films for almost a century, since their creation in 1891 [27].

Essential data can be inferred from the analysis of Langmuir isotherms such as structural phases and structural phase transitions. To obtain them experimentally, a Langmuir trough is used. The monolayer is initially deposited on top of the substrate. A moving barrier then closes in on the film and

the surface pressure (the difference between the surface tension of the subphase and the surface tension of the monolayer covered subphase) as well as the average molecular area are measured.

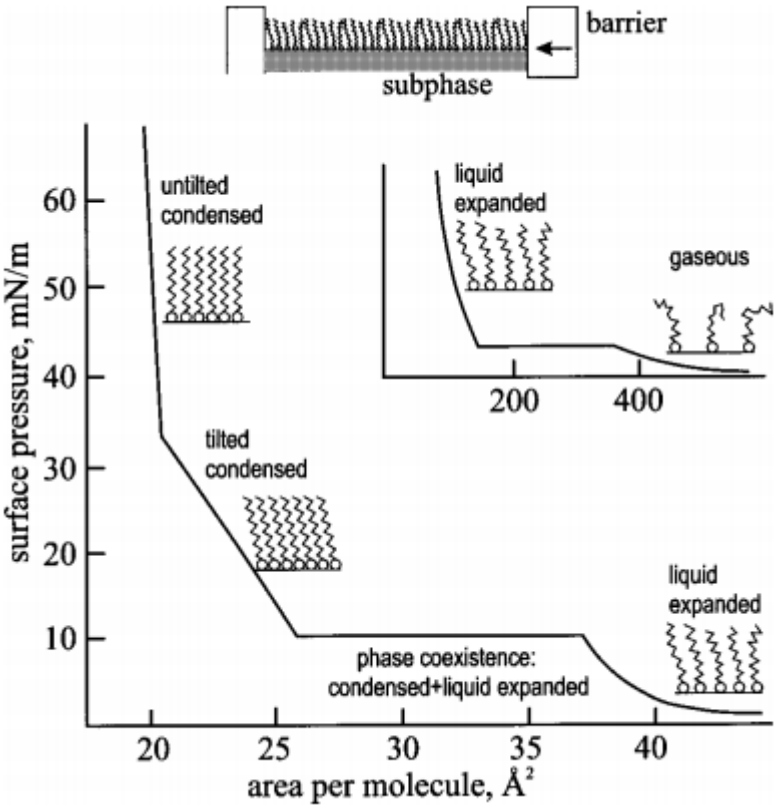

Figure 1 - Generalized Langmuir isotherm of a long chain hydrocarbon fatty acid. Adapted from [27].

As an example of a well characterized Langmuir isotherm, Figure 1 shows the surface pressure vs molecular area behavior for a long chain hydrocarbon fatty acid. It can be seen that, as expected, higher molecular areas correspond to higher disorder. For the Gaseous phase (G), the average molecular area is so high (400 $Å^2$) that the amphiphilic molecules can move freely, occurring low frequency encounters with weak intermolecular interactions. Therefore, at extremely low surface densities the film molecules behave as a 2D ideal gas.

As the system is compressed, this range is breached and a transition to a Liquid Expanded phase (LE) takes place. When the molecular area starts reaching the cross-sectional area of the monolayer molecules, further compression will cause the system to condense gradually in a first-order transition, originating a pressure plateau where there is simultaneously a LE phase and a (tilted) Condensed (C) phase [27]. It is noteworthy to say that this section is often not perfectly horizontal since this would imply that the system reaches equilibrium in every step, which experimentally is very difficult to achieve. Thermodynamic factors such as the tendency to form small molecular aggregates and surface micelles

[28] or kinetic ones, such as the moving barrier's speed, may interfere in the phase transitions and result in isotherms that deviate from what is represented in Figure 1.

After the coexistence plateau, all the film's molecules are in a "tilted condensed" phase, where the "tails" are tilted with respect to the water surface. This tilt characteristic is a response of the film molecules to increase intermolecular forces by maximizing the area of contact between fluorinated chains when molecular density is decreased [29]. Ultimately, the molecules have near-zero freedom of mobility at very high surface pressures, becoming virtually perpendicular to the water surface in a second-order transition, constituting an "untilted condensed" phase [27].

1.4. Molecular Dynamics Simulations

Molecular Dynamics simulations determine atomic positions over a previously set amount of time by solving Newton's classical equations of motion (Equation 1). With this data, trajectories over time can be calculated as well as quantitative predictions of several properties.

$$f_i = m_i \frac{\partial^2 r_i}{\partial t^2} = -\frac{\partial U}{\partial r_i} \quad (1)$$

The term f_i represents the net force applied in each particle i; U is the potential energy function, which is dependent on r_i, the position of each particle i.

The algorithm generally works as follows. First, the force is calculated for each particle. Then, Equation 1 is applied and acceleration is calculated. The velocity and, consequently, the position can thus be calculated taking into account the previous recorded position and a pre-set time-step.

In reality, to simulate real systems would be too computationally demanding. As a recourse, a representative subset (typically parallelepiped) is created and surrounded with virtual replicas of itself, hence acting as an infinite system. These system repetitions in every direction are named as periodic boundary conditions (PBC). If an atom goes through one of the box's boundaries, it shows on the opposite side with the same velocity. Since the simulation box behaves as a continuous medium, force calculations are not affected by this phenomenon.

The potential energy of each particle is the sum of intramolecular/bonded and intermolecular/non-bonded contributions, which are generally designated as the "force field". The functions and parameters used are obtained either from fitting to experimental data or quantum mechanics calculations.

According to the force field used in this work, OPLS-AA [30], the intramolecular interactions potential energy sum contains three terms: bond stretching, bond angle vibration (bending), and rotation of torsional (or dihedral) angles that revolve around equilibrium positions [31]. As Equation 2 depicts, the first two terms are harmonic potentials, while the dihedral angles term is a Fourier cosine truncated series. For computational efficiency reasons, the Ryckaert-Bellemans (RB) functional form (Equation 3) can be used instead of the latter term. The coefficients C_n can be calculated from the

Fourier coefficients $k_{ijkl}^{\phi,m}$ using the equalities in [32]. The RB functional form was the one used in the present work. A visual representation of the geometrical variables is shown below in Figure 2.

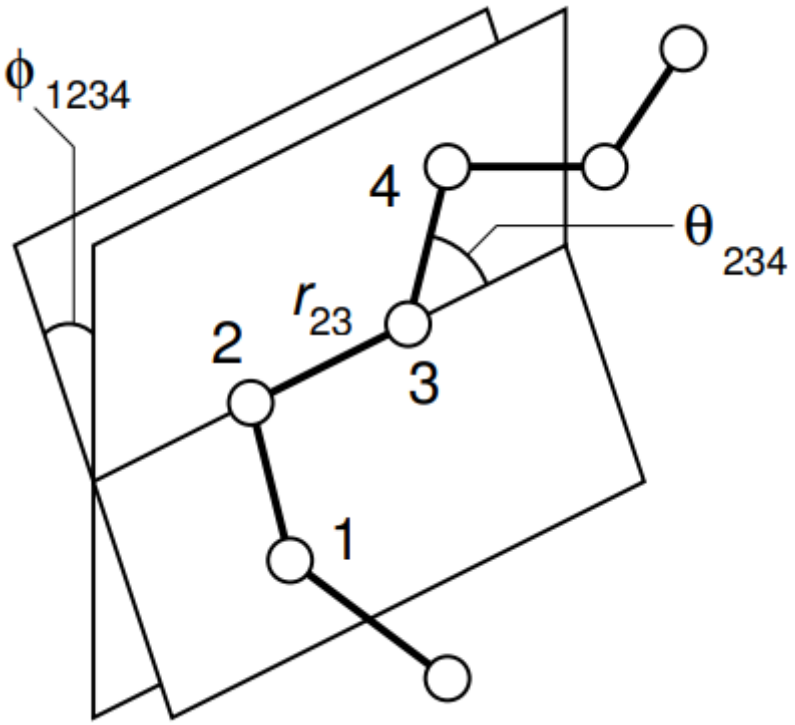

Figure 2 – Illustration of interatomic distance r_{23}, bend angle θ_{234}, and torsion angle ϕ_{1234} for a simple chain molecule. Adapted from [31].

$$u_{intramolecular} = \frac{1}{2}\sum_{\substack{bond\\stretch}} k_{ij}^{r}\left(r_{ij} - r_{eq}\right)^2 + \\ +\frac{1}{2}\sum_{\substack{angle\\vibration}} k_{ijk}^{\theta}\left(\theta_{ijk} - \theta_{eq}\right)^2 + \frac{1}{2}\sum_{\substack{torsion\\angles}}\sum_{m} k_{ijkl}^{\phi,m}\left(1 + cos\left(m\phi_{ijkl}\right)\right) \quad (2)$$

$$V_{rb}\left(\phi_{ijkl}\right) = \sum_{n=0}^{4} C_n(\cos(\psi))^n, \psi = \phi - 180º \quad (3)$$

The non-bonded interactions potential energy is the sum of the Lennard-Jones (LJ) term and Coulomb's Law, representing Van der Waals forces and electrostatic forces, respectively. The former describes the interaction between two atoms and consists of a repulsion term ($r_{ij}{}^{-12}$) and an attraction term ($r_{ij}{}^{-6}$). It is characterized by the zero-crossing distance, σ_{ij}, the inter-particle distance for which the potential is zero and the energy parameter, ε_{ij}, the minimum potential possible (Equation 4 and Figure 3). For heteronuclear interactions, both parameters are calculated through geometric mean combining rules between atom i and atom j (Equations 5 and 6).

$$u_{Lennard-Jones}(r_{ij}) = 4\varepsilon_{ij}\left[\left(\frac{\sigma_{ij}}{r_{ij}}\right)^{12} - \left(\frac{\sigma_{ij}}{r_{ij}}\right)^{6}\right] \tag{4}$$

$$\varepsilon_{ij} = \sqrt{\varepsilon_{ii}\varepsilon_{jj}} \tag{5}$$

$$\sigma_{ij} = \sqrt{\sigma_{ii}\sigma_{jj}} \tag{6}$$

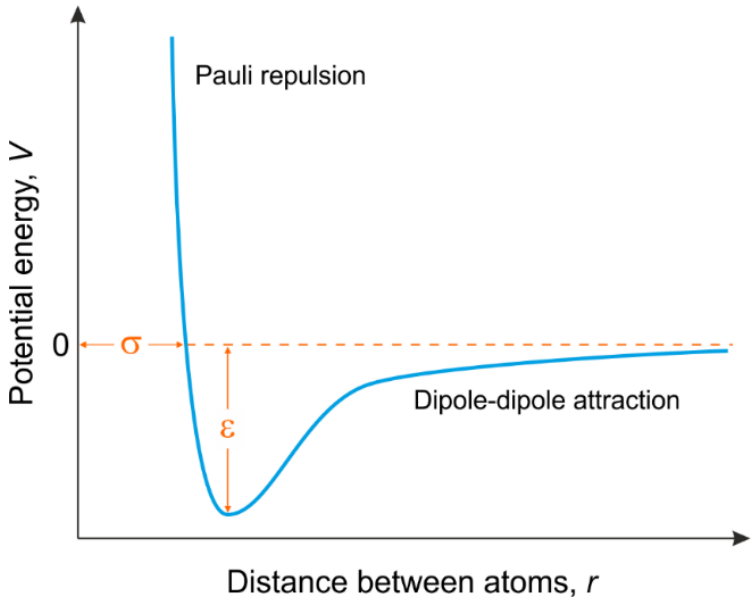

Figure 3 - Lennard-Jones potential function: Intermolecular potential energy as a function of the distance between a pair of particles. Adapted from [33].

Finally, the Coulomb energy is given by (Equation 7) and depends on the electrostatic charges of the particles (Q_i and Q_j) and the distance between them (r_{ij}).

$$u_{Coulomb}(r_{ij}) = \frac{Q_i Q_j}{4\pi\varepsilon_0 r_{ij}} \tag{7}$$

To increase computational efficiency, 3-body and higher order dispersive interactions are neglected, and the Lennard-Jones potential is parameterized in an effective manner in order to compensate this adjustment. In addition, long range intermolecular forces calculations with an inter-particle distance higher than a pre-set cut-off radius are computed through approximation methods.

2. Methodology

This chapter presents a description of the used software and its settings, simulation conditions, and fundamentals of the analysis made.

2.1. Molecular Dynamics Simulations

2.1.1. Software

The GROMACS 5.0.7 software package [34, 35, 36] was used to run the simulations and calculate most of the analysis' data. The Packmol software package (version 15.178) [37, 38] was used to compactly pack the amphiphilic molecules in cylindrical geometry. In addition, the systems' snapshots were obtained via the Visual Molecular Dynamics (VMD) software [39, 40].

Moreover, the order parameter and simulated GIXD spectra data were calculated using software recently developed by P. Lourenço [41]. The resulting properties were obtained based on Gaussian fitting with the Microsoft Office Excel software [42].

2.1.2. Simulation settings

All simulations ran at a temperature of 293.15 K in the NVT ensemble for at least 10 ns. The equilibration time was a minimum of 2 ns, which was determined based on the time it took for LJ and Coulomb energies to stabilize. The leap-frog algorithm was used to solve the equations of motion using a time-step of 2 fs. Additionally, the LINCS constraint algorithm was used for all bonds involving hydrogen atoms [43].

Furthermore, tri-directional periodic boundary conditions and V-Rescale thermostats were used [44]. A cut-off radius of 1.4 nm was set for intermolecular interactions, and for distances greater than this limit the Particle Mesh Ewald (PME) method was adopted to calculate long-range non-bonded forces. Since Coulomb's law is proportional to $r_{ij}{}^{-2}$, truncation errors have a particularly high negative impact in this interaction, making the use of this method essential. Because the simulated systems are highly anisotropic, the usual analytic tail corrections for the dispersive terms are not accurate and thus the PME method is also applied to the LJ potential.

2.1.3. Force Field

The used force field was based on the Optimised Potentials for Liquid Simulations – All Atoms (OPLS-AA) framework [30].

For the fluorinated molecules, the terminal group $–CF_2CH_2OH$ was modelled after the trifluoroethanol reported in [45] and [46], where the partial charge of the fluorinated carbon was adjusted to guarantee electrical neutrality. The remainder perfluoroalkyl chain follows the force field shown in [47], taking into account the reparametrization of the fluorine atoms charge (25% reduction to -0.150e)

and energy parameter (6% reduction to 0.208 kJ/mol), as described in [48]. As for the hydrogenated alcohols, the hydrogenated chain was modeled after L-OPLS [49] and the alcohol moiety after the original OPLS-AA parametrization [30]. Lastly, the water molecules are represented by the SPC/E three site rigid body model [50, 51]. The values used for the different parameters are fully detailed in Appendix A.

2.1.4. Initial Configurations

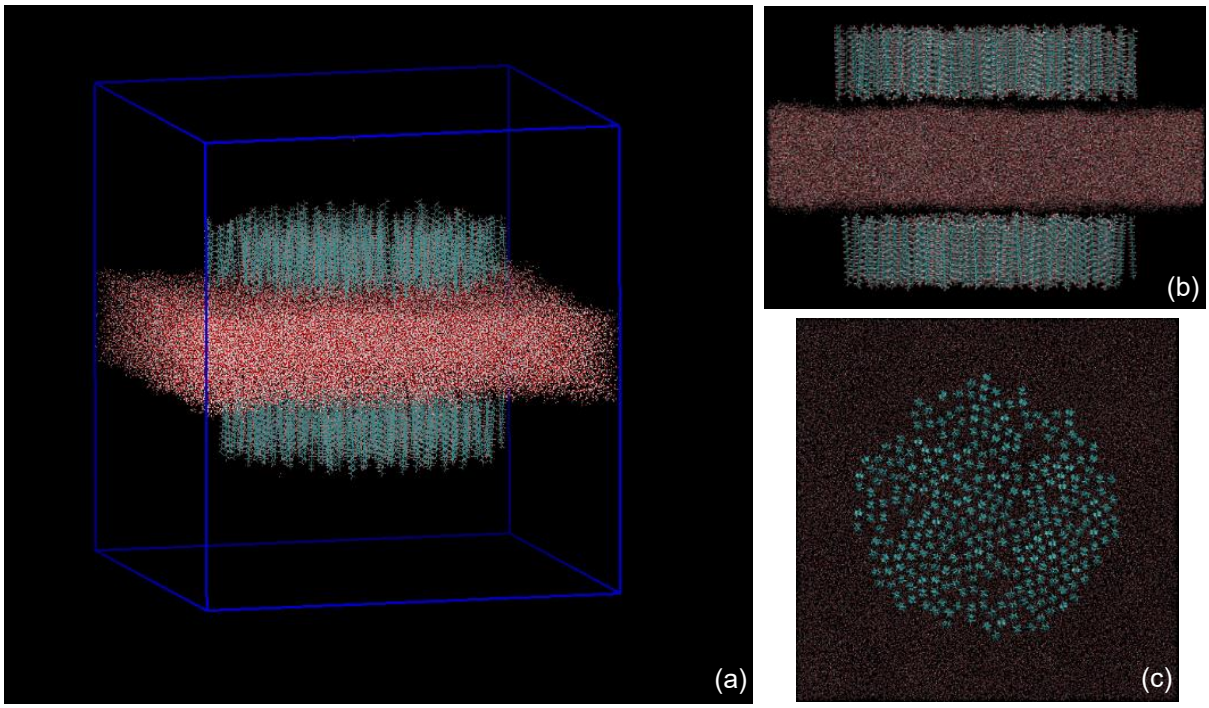

Figure 4 - (a) Exterior, (b) side and (c) top views of the initial starting configuration box for two monolayers of 300 F18OH molecules.

The Packmol software was used to densely pack the amphiphilic molecules in a cylindrical geometry as displayed in Figure 4(c), which accelerated the system's equilibration. Two aggregates were positioned in a box containing a pre-equilibrated water layer to better utilize the simulation box's space, with one film above and one below, and the alcohol group directed towards the water surface. A minimum thickness of 3 nm for the water slab was used to ensure there was no propagation of interaction effects from one monolayer side to the other.

Additionally, to avoid unintended interference through the periodic boundary conditions (PBC) via the z-axis, the simulation box's height was set at 20 nm. Special attention was also taken for the horizontal directions to ensure that aggregates from one box would not interact with adjacent replicas. In the initial configurations, it was made sure that the distance between the aggregate and the box's limits was higher than the cut-off radius to guarantee the inexistence of any artifacts resultant of non-bonded interactions or the unintended agglomeration of the amphiphilic molecules over the PBC.

All systems information is detailed in Appendix B by order of appearance in this text.

2.1.5. GIXD parameters

Several parameters that characterize the monolayer structure can be obtained by direct use of the information provided by GIXD spectra.

The effective molecular area $\langle A \rangle$, the real cross-sectional area that one molecule occupies within an ordered lattice was calculated according to Equation 8. Equation 9 was used to compute the hexagonal lattice parameter ($\langle d_{hk} \rangle$) and the coherence length l_c, which is the maximum distance for which the aggregate maintains a specified order degree, was determined as Equation 10 shows, which depends on the Full Width at Half Maximum (FWHM) for the sharpest peak.

$$\langle A \rangle = \langle d_{hk} \rangle^2 \cdot \frac{\sqrt{3}}{2} \tag{8}$$

$$\langle d_{hk} \rangle = \frac{2\pi}{Q_{hk,max}} \cdot \frac{2}{\sqrt{3}} \tag{9}$$

$$l_c = \frac{2\pi}{\mathrm{FWHM}} \tag{10}$$

2.1.6. Order Parameter

The Order Parameter (OP) is a computation that is used in this work to evaluate how aligned the molecules are relative to one another, giving a quantitative measure of organizational order in the films. It depends on the average of the dot product between all pairs of end-to-end vectors and is defined as follows:

$$OP = \frac{2}{N(N-1)} \sum_{i=1}^{N-1} \sum_{j>i}^{N} \frac{\vec{r}_i(t) \cdot \vec{r}_j(t)}{\|\vec{r}_i(t)\| \cdot \|\vec{r}_j(t)\|} \tag{11}$$

Where $\vec{r}_{i,j}$ are the molecular vectors between the carbon bonded to the alcohol group and the terminal carbon, $\|\vec{r}_{i,j}\|$ is the modulus of the molecular vector and N is the number of alcohol molecules in the simulation box. If the molecules are perfectly parallel relative to one another, OP assumes the value of 1, which lowers the more disorganized the system is.

3. State of the Art

Due to the fluorocarbons higher chain stiffness, perfluorinated alcohols and perfluorinated fatty acids behave differently from the generic hydrocarbon curve (Figure 1). When these types of compounds have between one or two CH_2 spacers (H-spacer), they exhibit identical isothermic behavior [52, 53, 15]. That said, for the purpose of referencing and comparison with literature, these compounds will be treated as equivalents.

Some of the findings of this work were recently published together with experimental observations in [53]. This text presents a more complete view of the MD simulation work, expanding on the published results. Key experimental data on the studied systems are shown below, providing the context for the present dissertation.

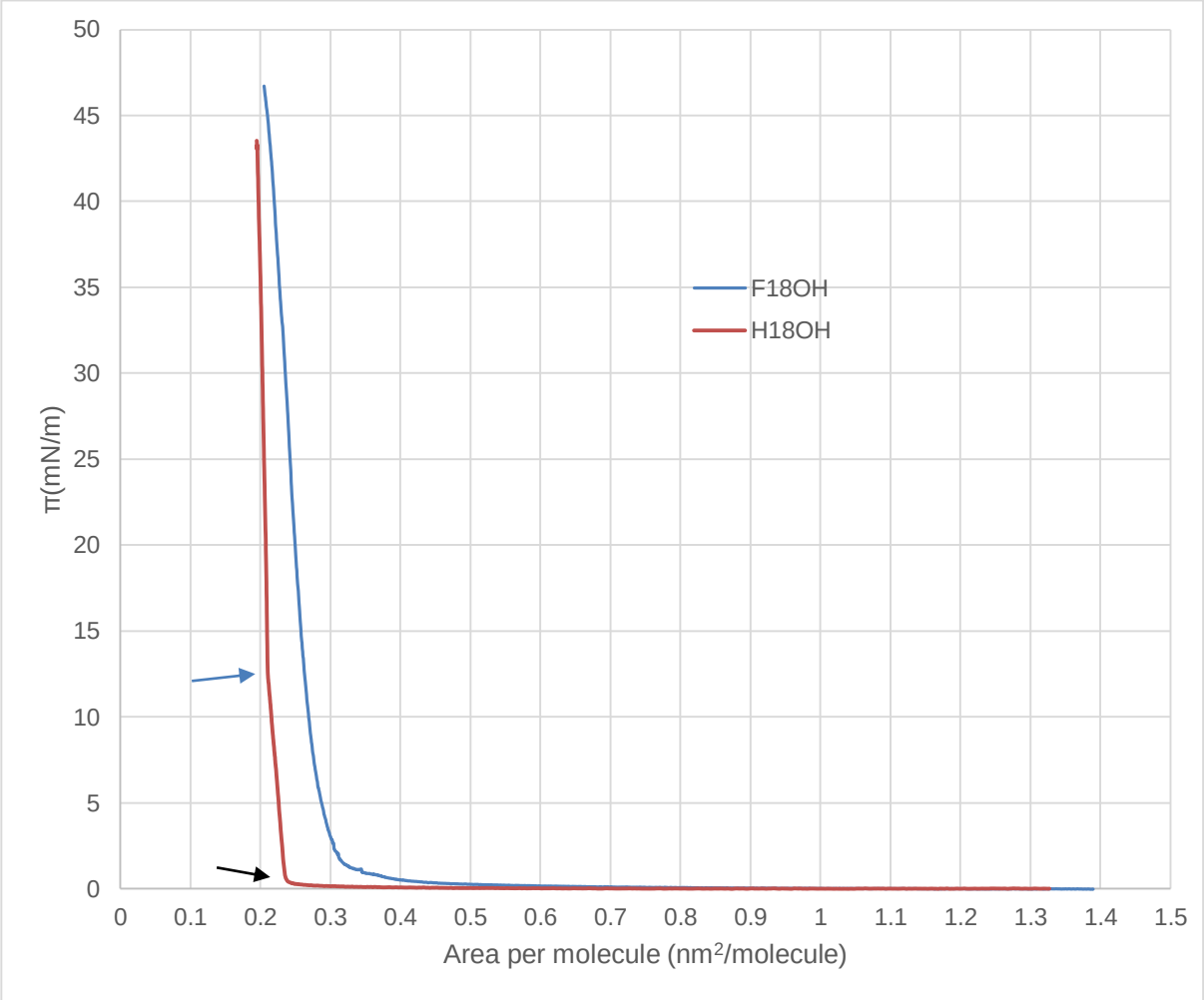

Figure 5 - Experimental Langmuir isotherms of F18OH and H18OH systems at 293.15 K. Data provided by [53].

As displayed in Figure 5, it can be seen that H18OH shows identical behavior to the generic hydrocarbon amphiphile isotherm shown in Figure 1. By analogy, the isotherm of H18OH can be interpreted in the following way. Starting from the highest molecular areas (A = 1.3 nm^2/molecule) a

plateau of coexistence between a condensed and liquid expanded phases (LE+C) can be seen. The first “kink” indicated by the black arrow represents the end of the plateau, after which only a tilted condensed phase is present, which converts into an untilted condensed phase in a second-order transition. The second “kink”, represented by the blue arrow, indicates the end of this transition.

As for the F18OH curve, a plateau is shown from very high molecular areas (~1.2 nm^2/molecule) until close to the value of 0.3 nm^2/molecule, the characteristic cross-sectional area of perfluoalkane molecules. At this point, when the monolayer becomes increasingly denser, a lift-off occurs. This suggests the existence of a condensed phase for very low molecular areas, which coexists in the plateau range with a gaseous phase [53]. This behavior has also been experimentally proven to take place for short-chain perfluorinated fatty acids and alcohols with up to 2 H-spacers [15, 52, 16, 54, 55].

Atomic Force Microscopy (AFM) data for F14OH and F18OH was obtained in 2014 by M. Teixeira [56] and was recently published in [53].

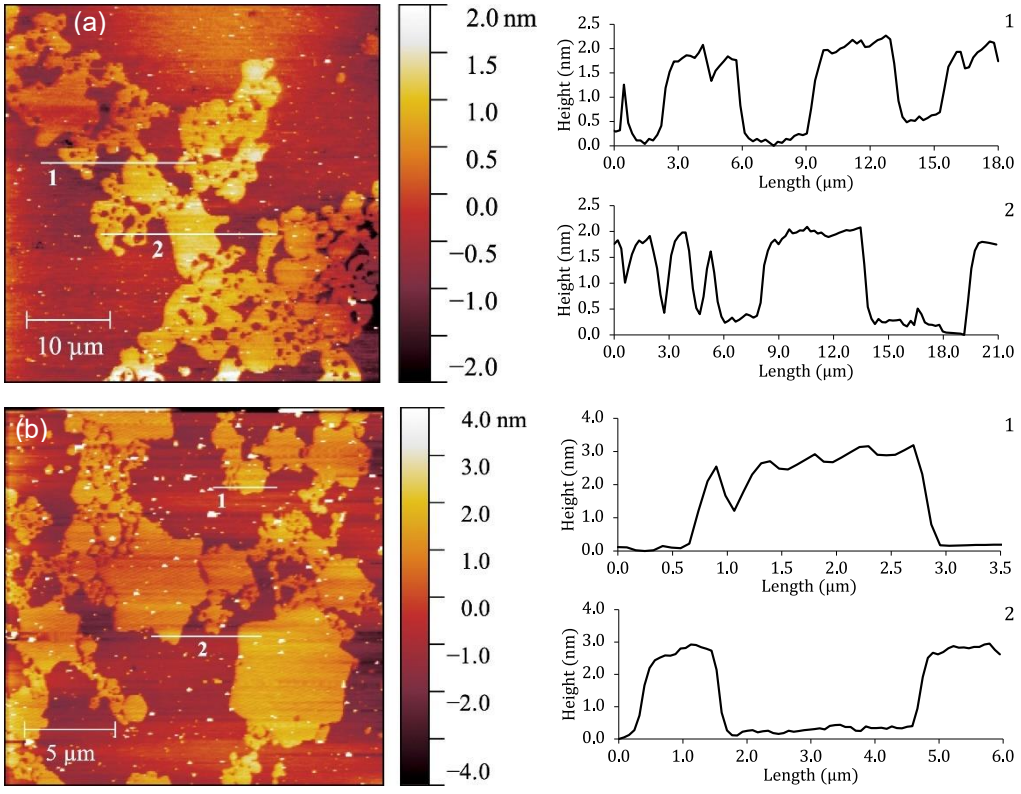

Figure 6 - AFM height images of (a) F14OH at 0.7 nm^2/molecule, (b) F18OH at 0.85 nm^2/molecule. The right panels show the height profiles along the numbered lines on the AFM images. Adapted from [53].

Figure 6 shows AFM images of F14OH (Figure 6(a)) and F18OH (Figure 6(b)) Langmuir films at large area per molecule values, located in the near-zero surface pressure plateau. For both systems, the existence of 2D solid-like aggregates is clear. F14OH aggregates are presented as a network of round-edged filaments and the F18OH films as hexagonal or star-shaped structures. These results are

distinct from what happens for the hydrogenated alcohols, since these tend to coalesce in liquid domains, producing a smooth and homogeneous surface [56].

The described discrepancies between the behavior of the hydrogenated alcohols and their perfluorinated equivalents are the motivation behind this study, which seeks to further characterize the Langmuir monolayers comprised of these molecules at a molecular scale.

4. Molecular Dynamics Simulations Results and Discussion

4.1. Gas Phase

Several MD simulations were performed at very high molecular areas to evaluate if a gas phase could be identified in the simulations. The onset of a stable aggregate was found to be between the systems of 10 molecules and 5 molecules for 18.2 nm side boxes, at molecular areas of 33.1 nm^2/molecule and 66.2 nm^2/molecule, respectively. The behavior of the second system was distinct from the first since the molecules attached and detached from each other frequently, and the loose monomers would scatter along the surface, whereas in the first a cluster was maintained throughout the simulation. Snapshots are shown in Figure 7.

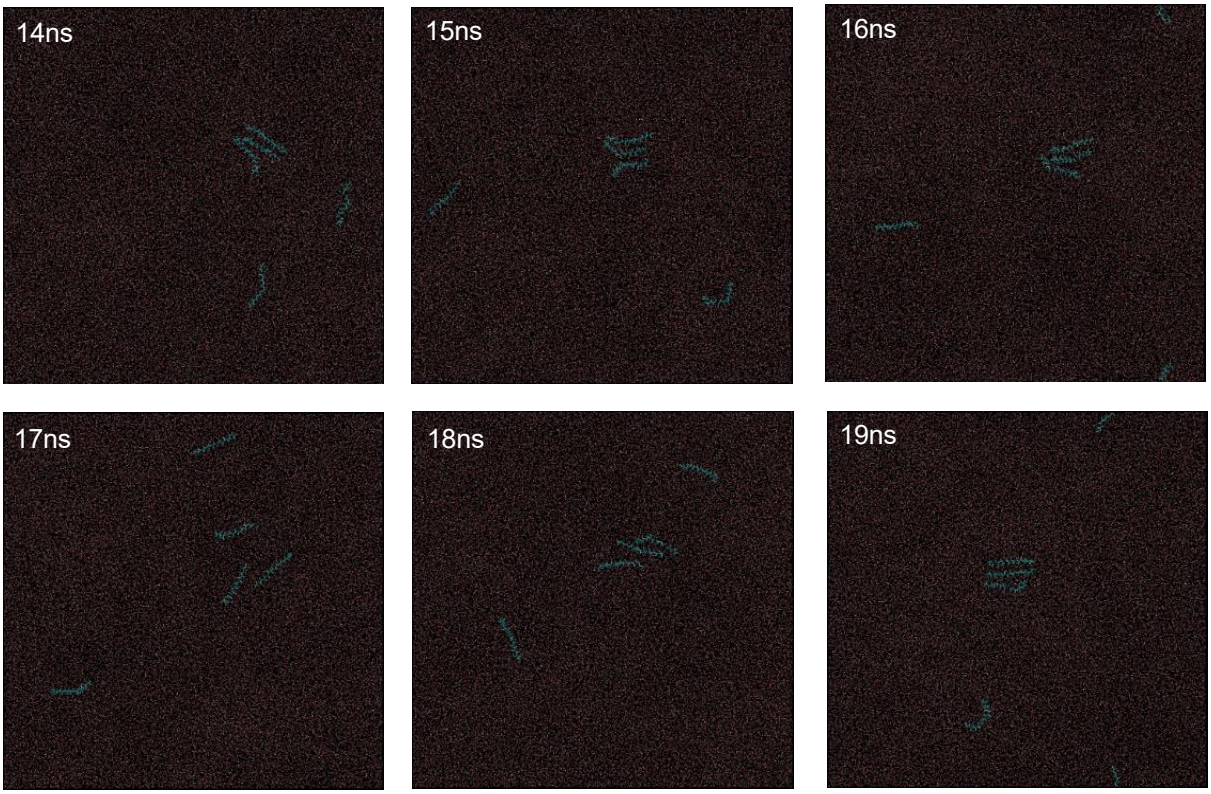

Figure 7 – Top view simulation snapshots over 6 ns of production time for a 5 molecule F18OH monolayer system in a 18.2 nm side box, at a molecular area of 66.2 nm^2/molecule.

As shown in the figure above, the aggregate does not seem to be ordered or stable since its molecules are laid down and show a low contact area between them. As a result, some units often disaggregate and move freely throughout the water surface, resembling a gaseous phase.

4.2. Impact of the Aggregate's Size

Several systems along the π = 0 mN/m plateau containing different numbers of F18OH molecules were studied by calculating molecular tilt and dihedral angle distributions, in addition to the average order parameter. Trajectory snapshots were also added to complement and better understand these results, giving visual representation of the molecules' movement during the simulation.

4.2.1. Molecular Tilt Distribution

Each molecule is characterized by a vector between the carbon linked to the alcohol group and the terminal carbon. The tilt angle, defined as the angle between this vector and the normal to the water surface, can then be calculated. This calculation is repeated for every molecule in every recorded configuration, and a probability distribution of tilt angles is determined. For a systematic and facilitated understanding of the presented figures, the type of legend shown in the figure below is always written as follows: "base molecule of the system" "number of alcohol molecules" "molecular area" "length of the box side".

Figure 8, shown below, presents the tilt angle histograms for six F18OH systems of different sizes, calculated based on a production time of 8 ns through 8000 equally spaced frames. Snapshots from representative systems are shown in Figure 9-Figure 12.

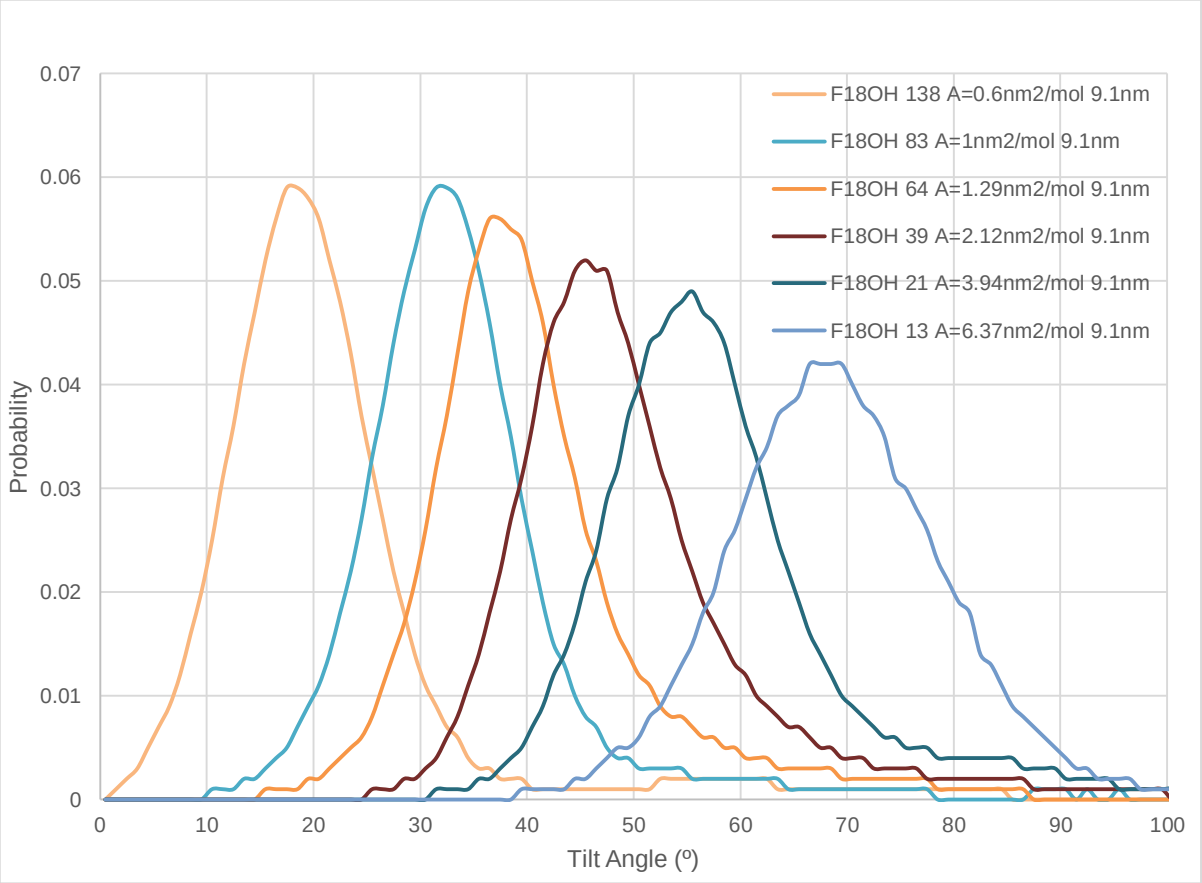

Figure 8 - Probability vs Tilt Angle for F18OH systems with different number of molecules in 9.1 nm side boxes.

Figure 8 shows that the fewer the molecules of F18OH, the broader the bell curve and higher the standard deviation and the medium value for the tilt angle are. The evolution of the tilt angle indicates that molecules from the smaller aggregates mainly lay down on the water surface while in bigger systems they tend to position themselves in parallel to the z-axis. As for the standard deviation progress, it shows that the bigger the aggregate's size, the less freedom the molecules have to adopt different positioning. Taking this into consideration it can be stated that the more F18OH molecules constitute the aggregate, the more the individual movement of the units is restricted, resulting in stiffer and more stable Langmuir films, and closer to being perpendicular to the water surface.

The trajectory snapshots can further enrich these assessments. Judging by Figure 10-Figure 12, presented below, the molecules seem to have less chain flexibility and mobility the bigger the aggregate is, leading to a decrease of the standard deviation, which is why a narrowing of the curve is seen with the increase of the number of molecules in the system. This stems from the strengthening of intermolecular cohesion as the number of molecules increases and the total area stays the same. It can also be seen that one side of the aggregates sinks more into the water line than the other. This strengthens amphiphile-water intermolecular interactions, reaching an energy minimum that amphiphile-amphiphile non-bonded forces do not accomplish. This effect is more visible for the smaller aggregates.

In extremely low surface density cases, like the one represented in Figure 9, the molecules tend to stack almost horizontally, sometimes in a 3 molecule layer (middle group at 8.5 ns). It is important to note that the alcohol groups never leave the water surface, reflecting the head's strong hydrophilicity. In contrast, the tail's hydrophobicity is such that the fluorocarbon chain stays aggregated to the ones of other molecules even if it has to virtually fold on itself, as shown by the first molecule on the right from 9ns (b).

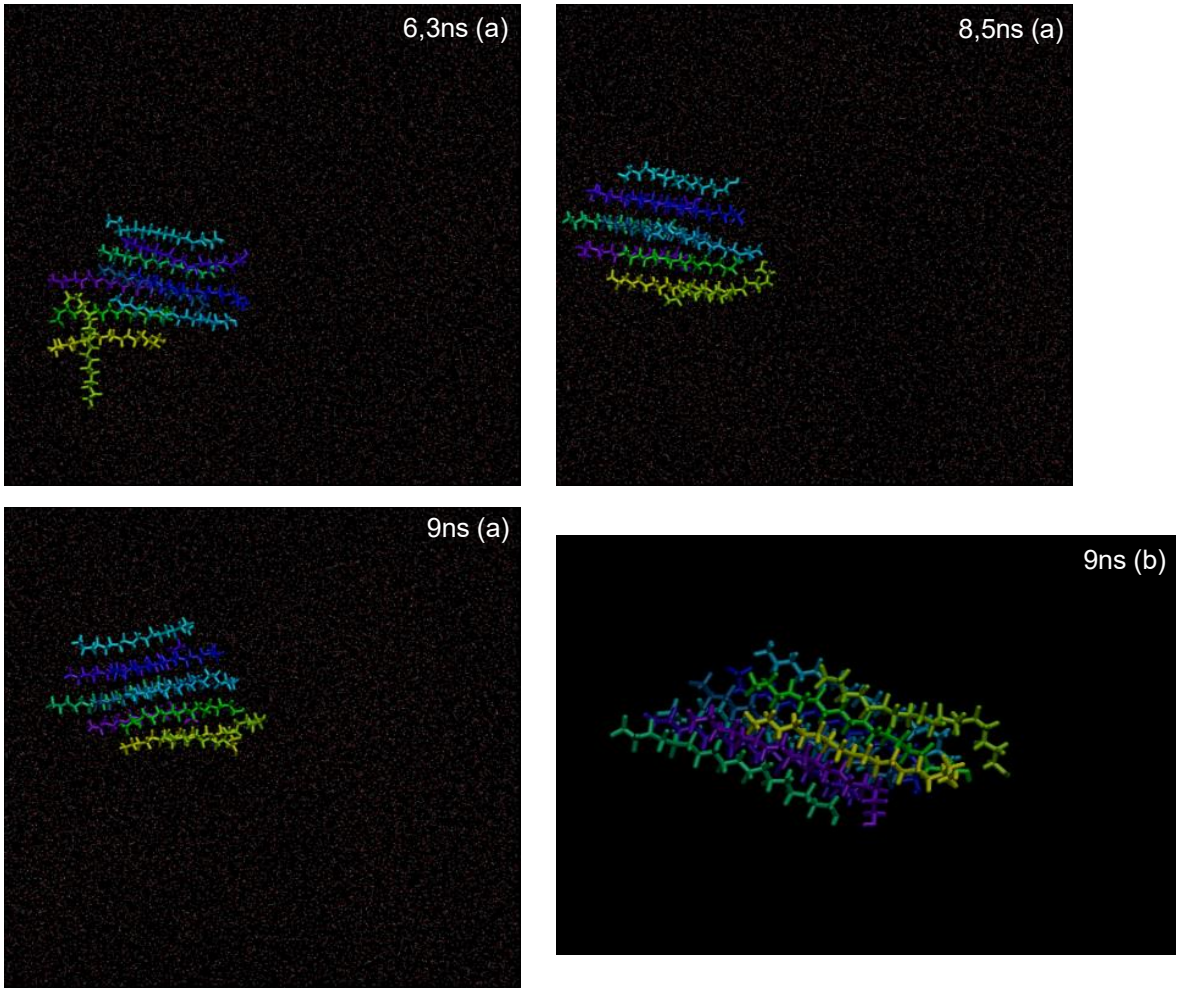

Figure 9 - (a) Top and (b) side views simulation snapshots for the system of 10 F18OH molecules, at a molecular area of 8.28 nm^2/molecule (9.1 nm side box). The water molecules were eliminated from image (b) in order to see the alcohol molecules more clearly.

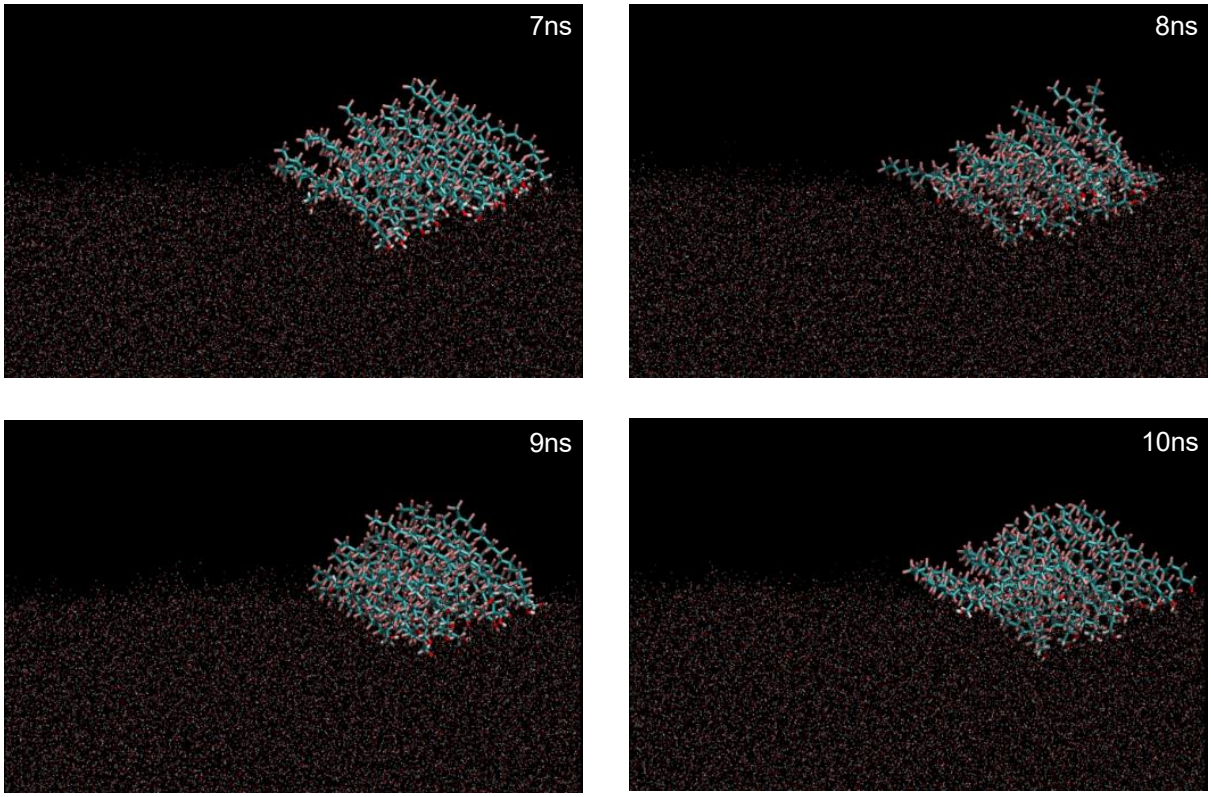

Figure 10 – Side view simulation snapshots over 4 nanoseconds of production time for the 21 F18OH molecule monolayer system referred in Figure 8.

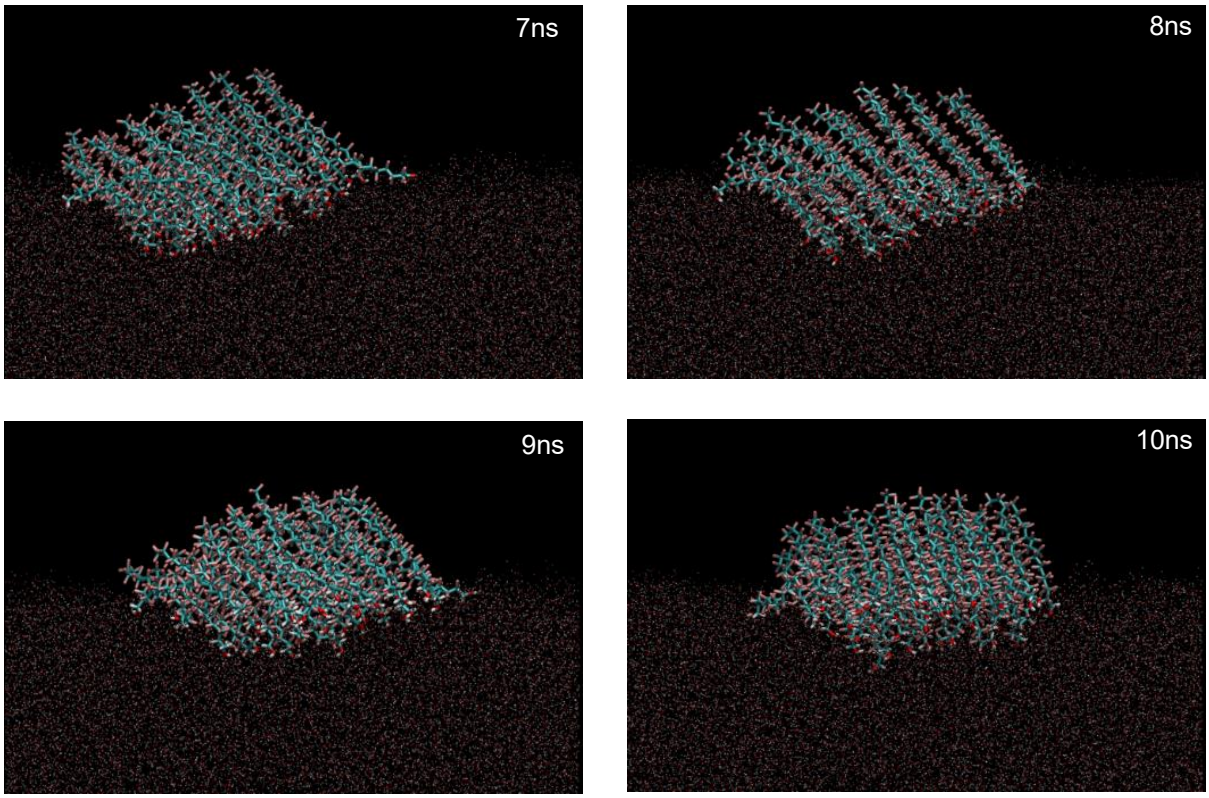

Figure 11 – Side view simulation snapshots over 4 nanoseconds of production time for the 39 F18OH molecule monolayer system referred in Figure 8.

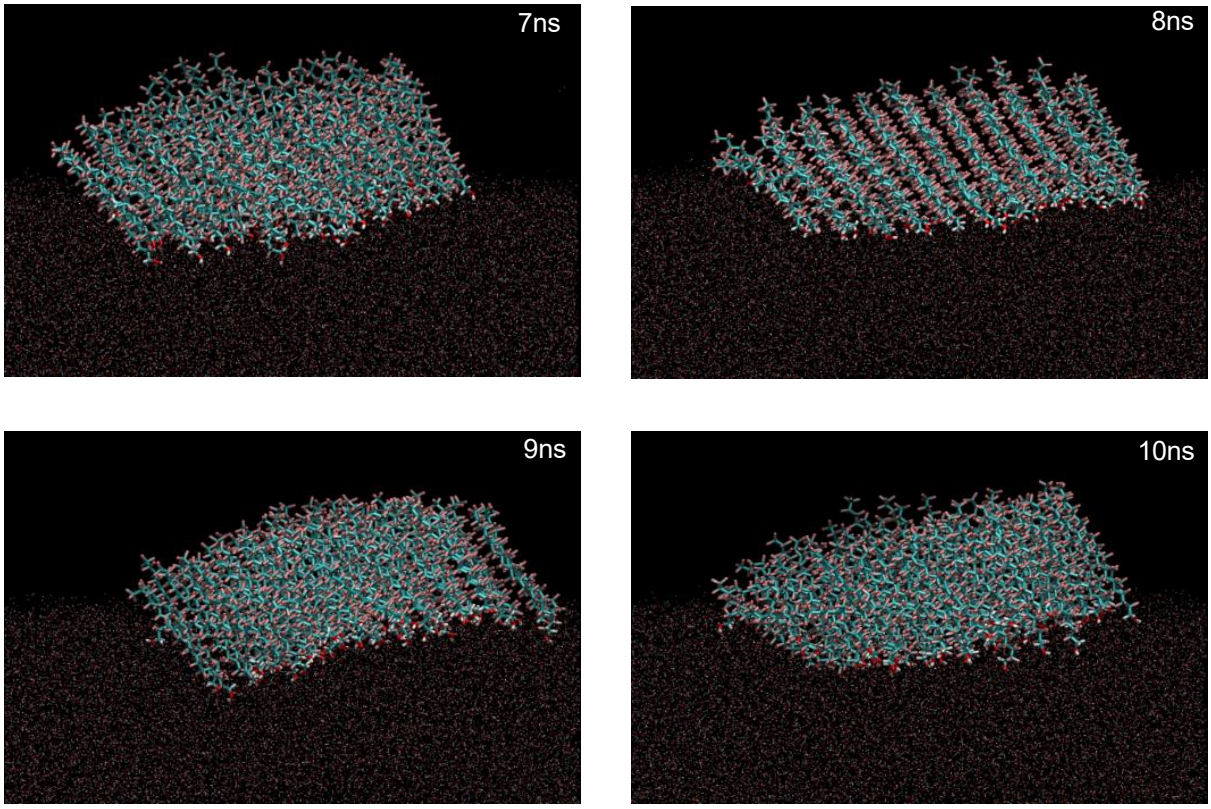

Figure 12 - Side view simulation snapshots over 4 nanoseconds of production time for the 83 F18OH molecule monolayer system referred in Figure 8.

4.2.2. Order Parameter

The order parameter (OP) was also calculated for these systems. As previously mentioned in 2.1.6, this computation measures how parallel the molecules are relative to one another by using the same end-to-end vector as the tilt angle analysis. If all the system molecules are perfectly aligned with each other, the OP assumes the value of 1. It was calculated by block averaging 8 ns of production time in 2 ns intervals.

The average order parameter for the recurrent F18OH systems set is shown below, in Figure 13.

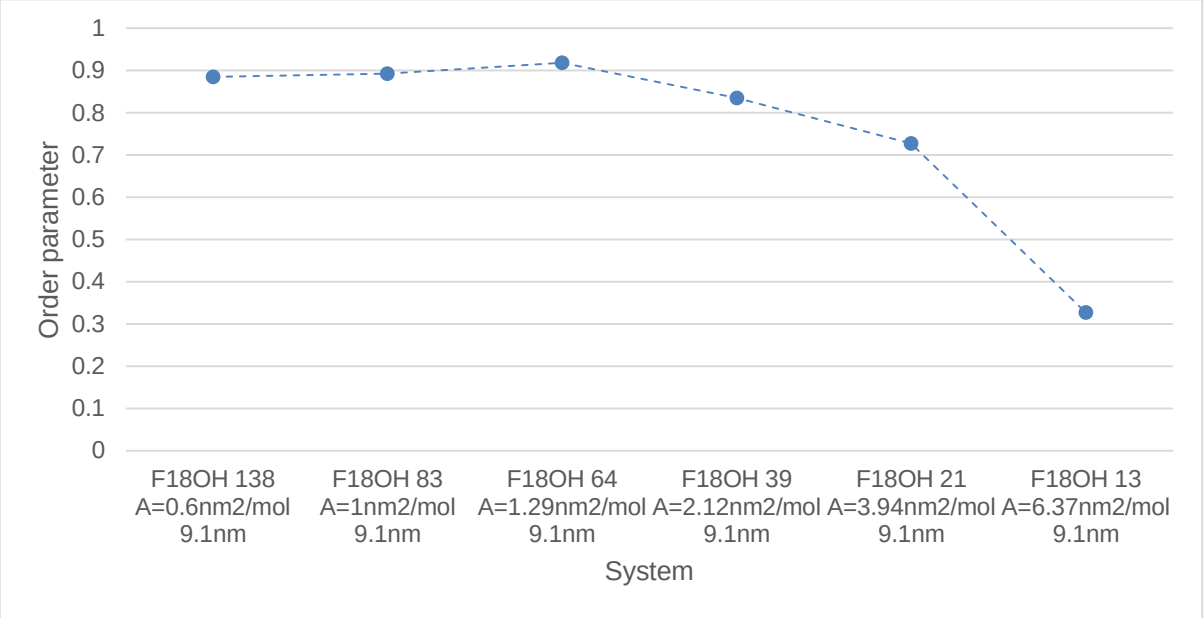

Figure 13 - Average Order Parameter (⟨OP⟩) for F18OH systems of different scale.

In line with what was verified in the tilt angle analysis, the systems become more disordered with the decrease of the aggregate's size. The 64 molecule monolayer seems to be above the critical size limit, after which the molecules are essentially parallel for all systems.

More information was obtained from the analysis of the trajectories development. With the decrease of the number of F18OH molecules, the higher is the percentage of molecules in the periphery of the aggregates that tend to leave it or lay down over time, creating a more significant disassembly effect (from the rim to the center) than it would in bigger aggregates. Also, smaller aggregates free up more space in the simulation box and, consequently, molecules that disaggregate take more time to return to the aggregate, resulting in a higher degree of disorder over time; this is well represented in Figure 14 by the blue colored F18OH molecule movement.

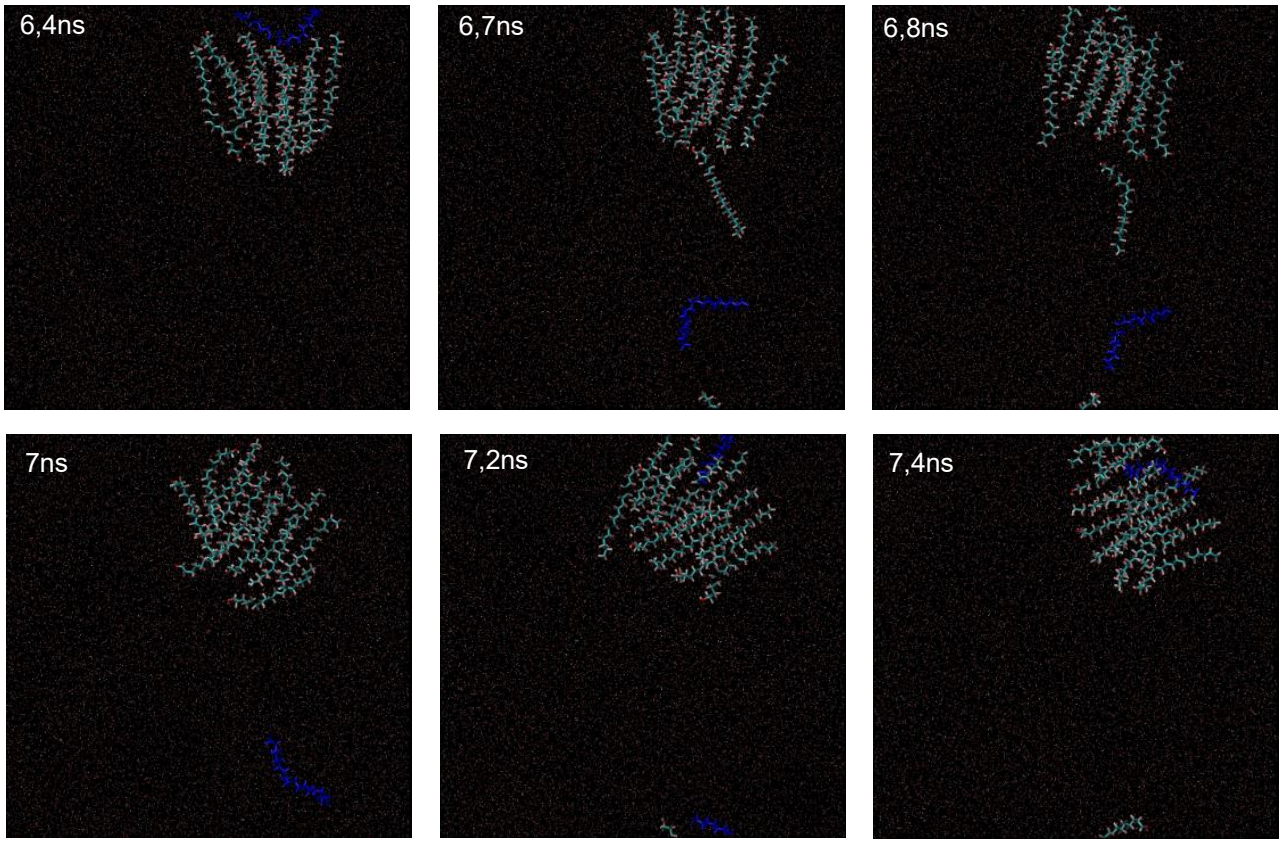

Figure 14 – Top view simulation snapshots over 1 nanosecond of production time for the 13 F18OH monolayer system referred in Figure 8.

4.2.3. Dihedral Angle Distribution

In order to better understand the atom arrangements for different systems and conditions, dihedral angle distributions for C-C-C-C bonds of the fluorinated chain were calculated, as well as the probability densities for the *gauche* and *trans* conformations. The results for the same six different F18OH films are exhibited below, calculated over 8 ns of production time and 8000 equally spaced frames.

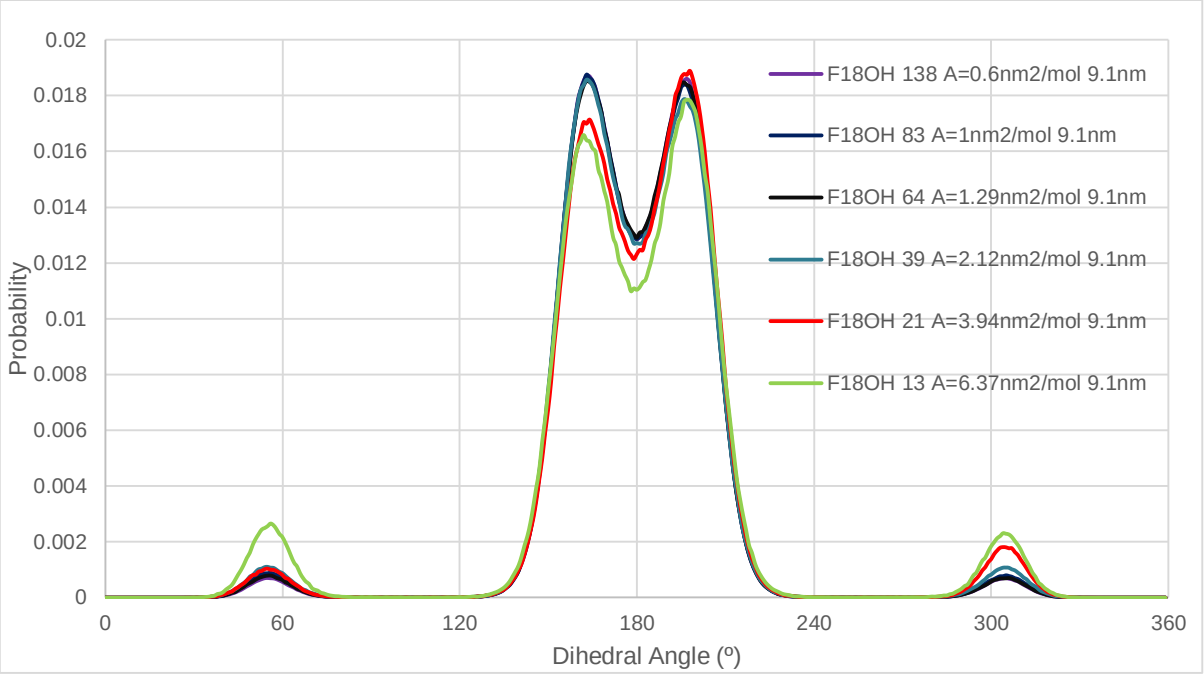

Figure 15 - Probability vs Dihedral Angle for F18OH systems with different number of molecules in 9.1 nm side boxes.

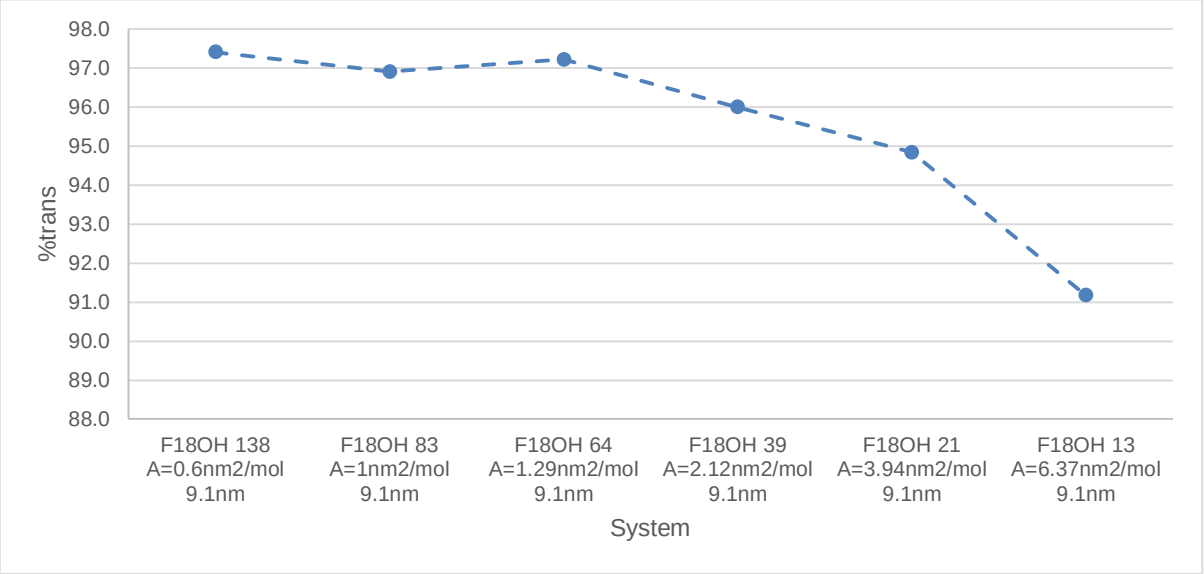

Figure 16 - *Trans* conformation probability density for the systems shown in Figure 15. *Gauche* and *trans* correspond to dihedral angle ranges of [0º,119º]∪[240º,359º] and [120º,239º], respectively.

The graphical analysis of Figure 15 shows that the (slightly distorted) *trans* arrangement is highly favored over the *gauche* one. Individually, most systems are shown to be inclined to one of the sides of the rotation ([0º,119º] vs [240º,359º] for the *gauche* conformation and [120º,179.5º] vs [179.5º,239º] for the *trans* conformation). However, an overview shows that this inclination changes for the different systems with no apparent tendency. Also, the difference in probability for the equivalent rotations diminishes with the increase of the molecules' body size, making it reasonable to conclude that this occurrence is most likely due to randomized partiality given the limited number of molecules in the simulated aggregates.

Additionally, Figure 16 demonstrates that the percentage of dihedral angles in *trans* conformation increases with the aggregate size, demonstrating that the *gauche* arrangement is gradually more suppressed the bigger the monolayer is. Since it was learned from the preceding analysis that smaller aggregates are disordered and have more laid down molecules, and that *gauche* defects negatively affect the organization of films, it is likely that the majority of the percentage of these defects come from tilted or laid down molecules.

Besides, it is very interesting to note that this graphical behavior is identical to the one of the order parameter presented in Figure 13. This may be evidence that these properties are correlated and that the adoption of *trans* configurations among the chain carbons is needed to produce ordered and stable domains.

4.3. Influence of Chain Length

In this section, systems of F18OH, F16OH, F14OH, F12OH and their hydrogenated counterparts, located in the near-zero surface pressure plateau, are approached. In first place, snapshots are presented, followed by molecular tilt distributions, order parameter analysis, dihedral angle distribution and simulated GIXD spectra vs experimental GIXD data analysis.

4.3.1. Snapshots

In Figure 17-Figure 20, represented below, are snapshots of 550 molecule systems of every studied compound. These images will often be referred to later in this text to complement and better understand the quantitative analysis.

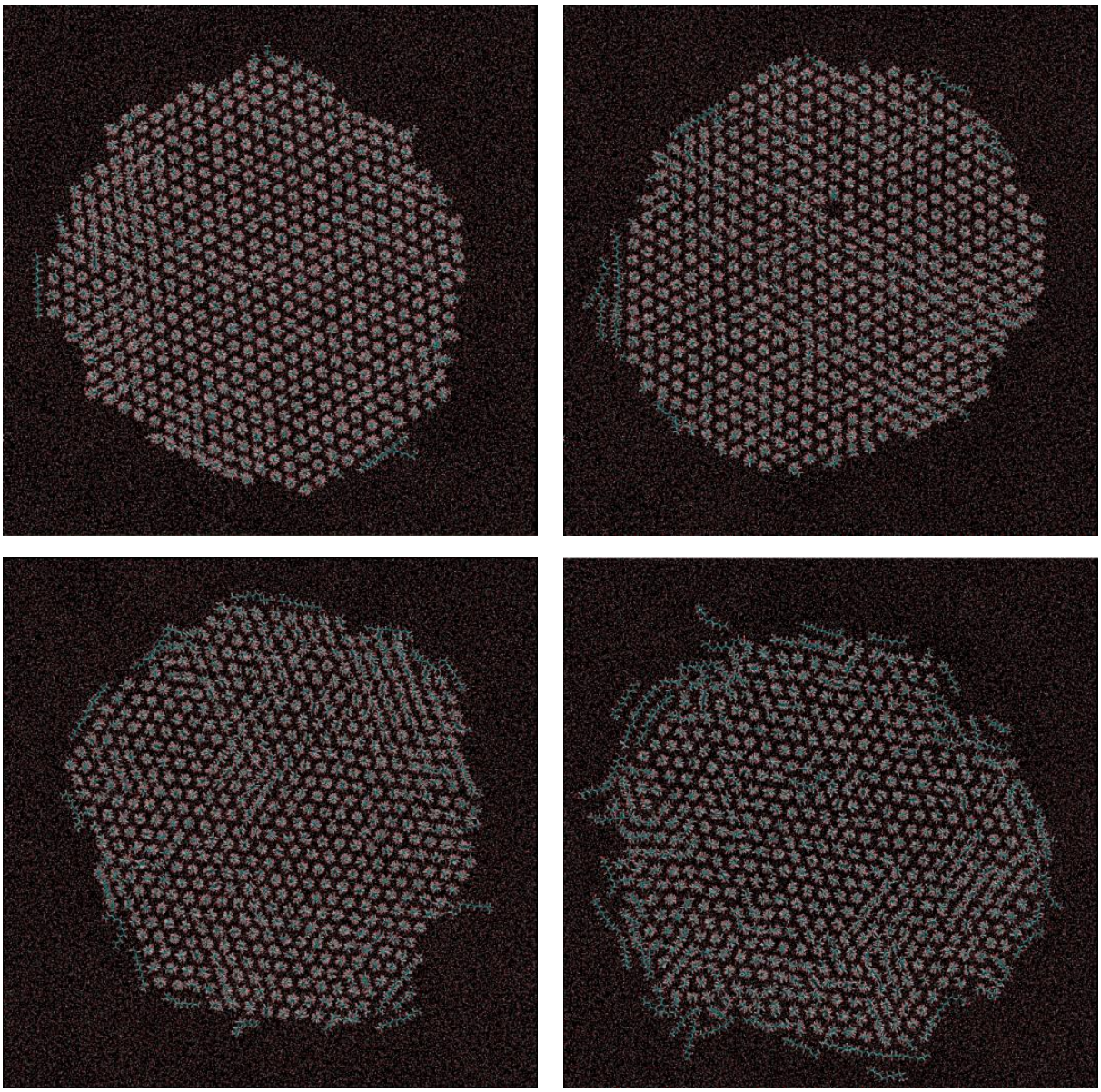

Figure 17 - Top view simulation snapshots of F18OH, F16OH, F14OH and F12OH systems (left to right), after 10 ns of simulation time. All boxes contain 550 amphiphile molecules at a molecular area of 0.6 nm^2/molecule (18.2 nm side box).

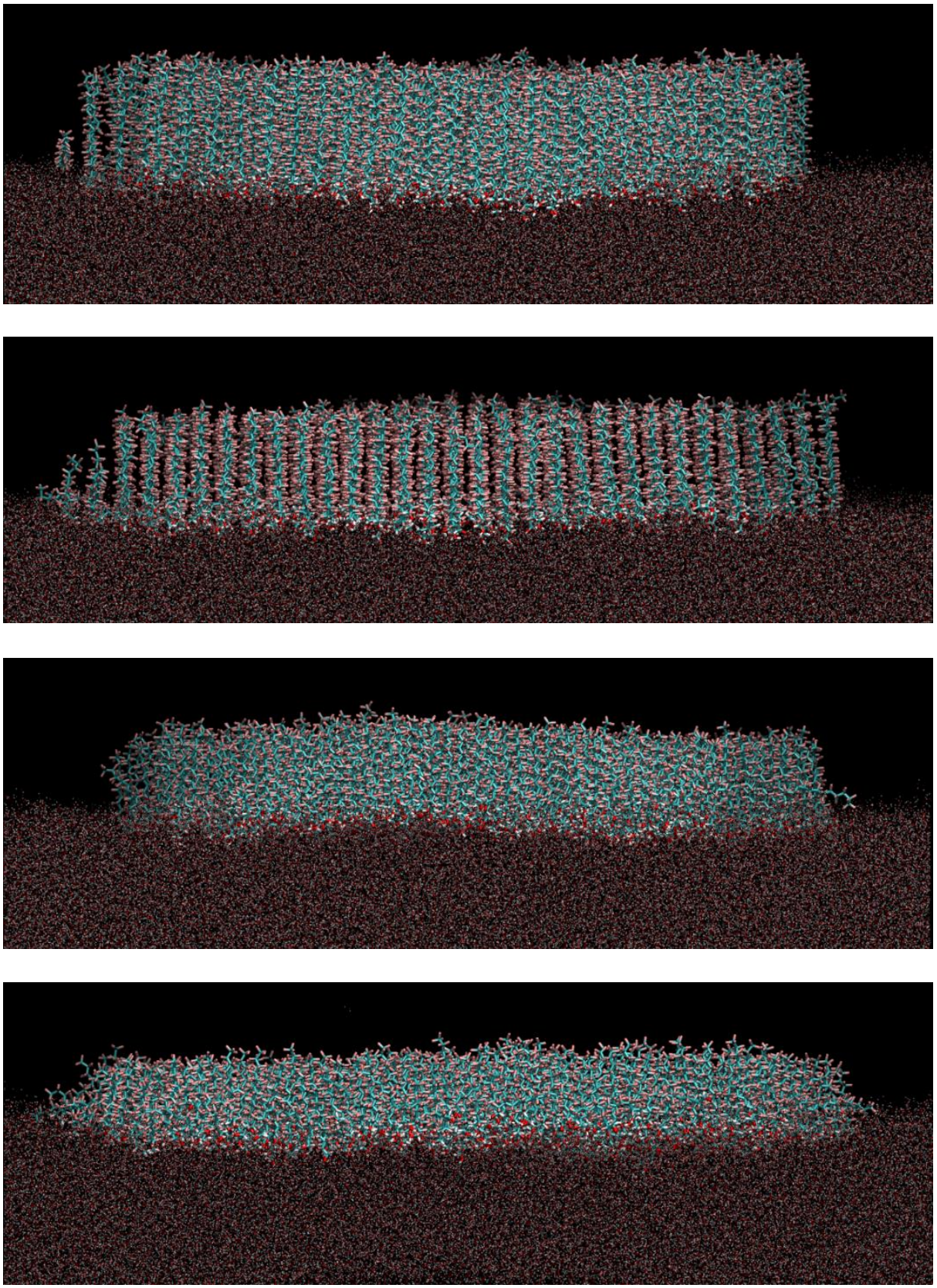

Figure 18 - Side view simulation snapshots of F18OH, F16OH, F14OH and F12OH systems (top to bottom), after 10 ns of simulation time. All boxes contain 550 amphiphile molecules at a molecular area of 0.6 nm^2/molecule (18.2 nm side box).

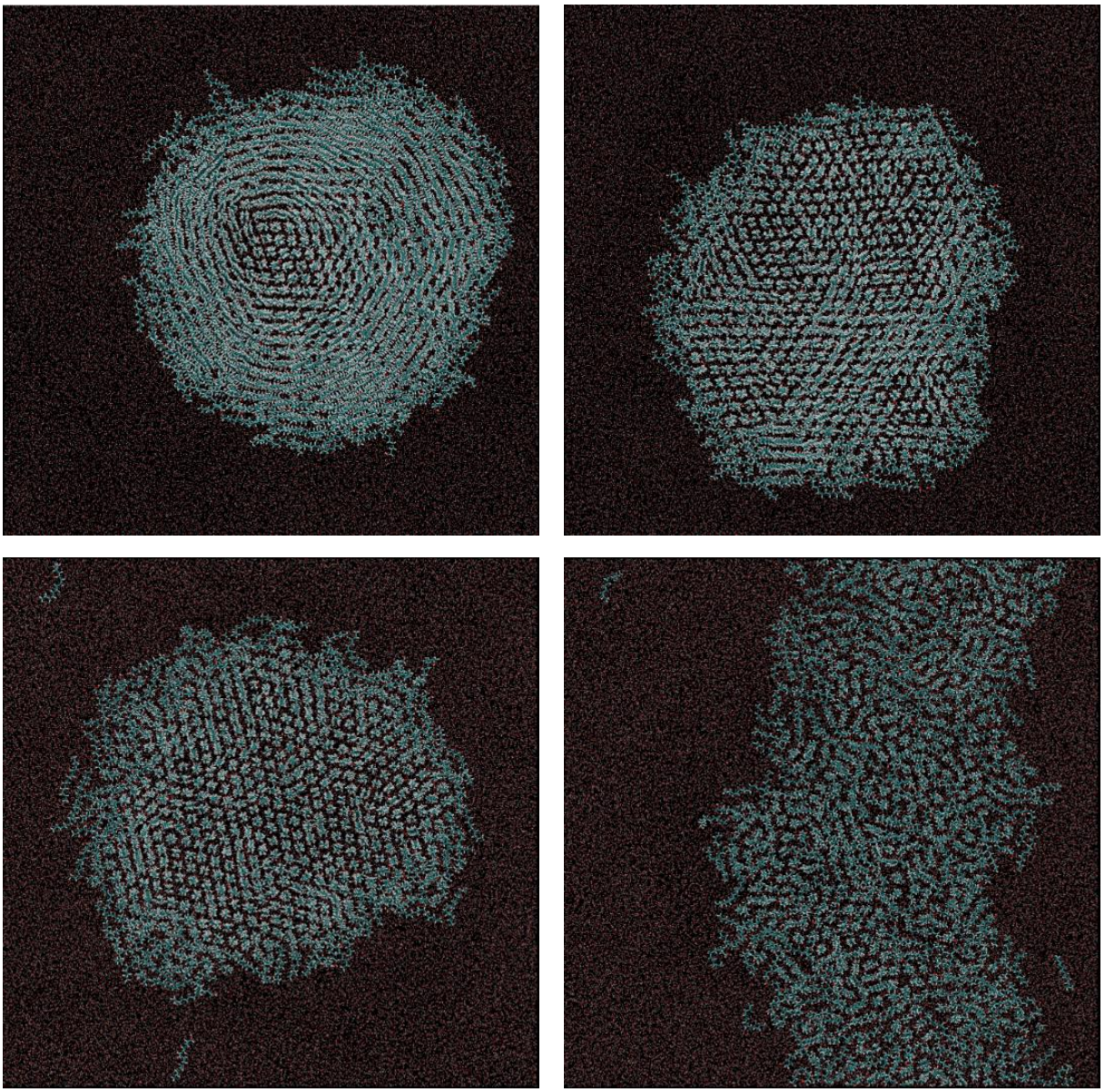

Figure 19 - Top view simulation snapshots of H18OH, H16OH, H14OH and H12OH systems (left to right), after 10 ns of simulation time. All boxes contain 550 amphiphile molecules at a molecular area of 0.6 nm^2/molecule (18.2 nm side box).

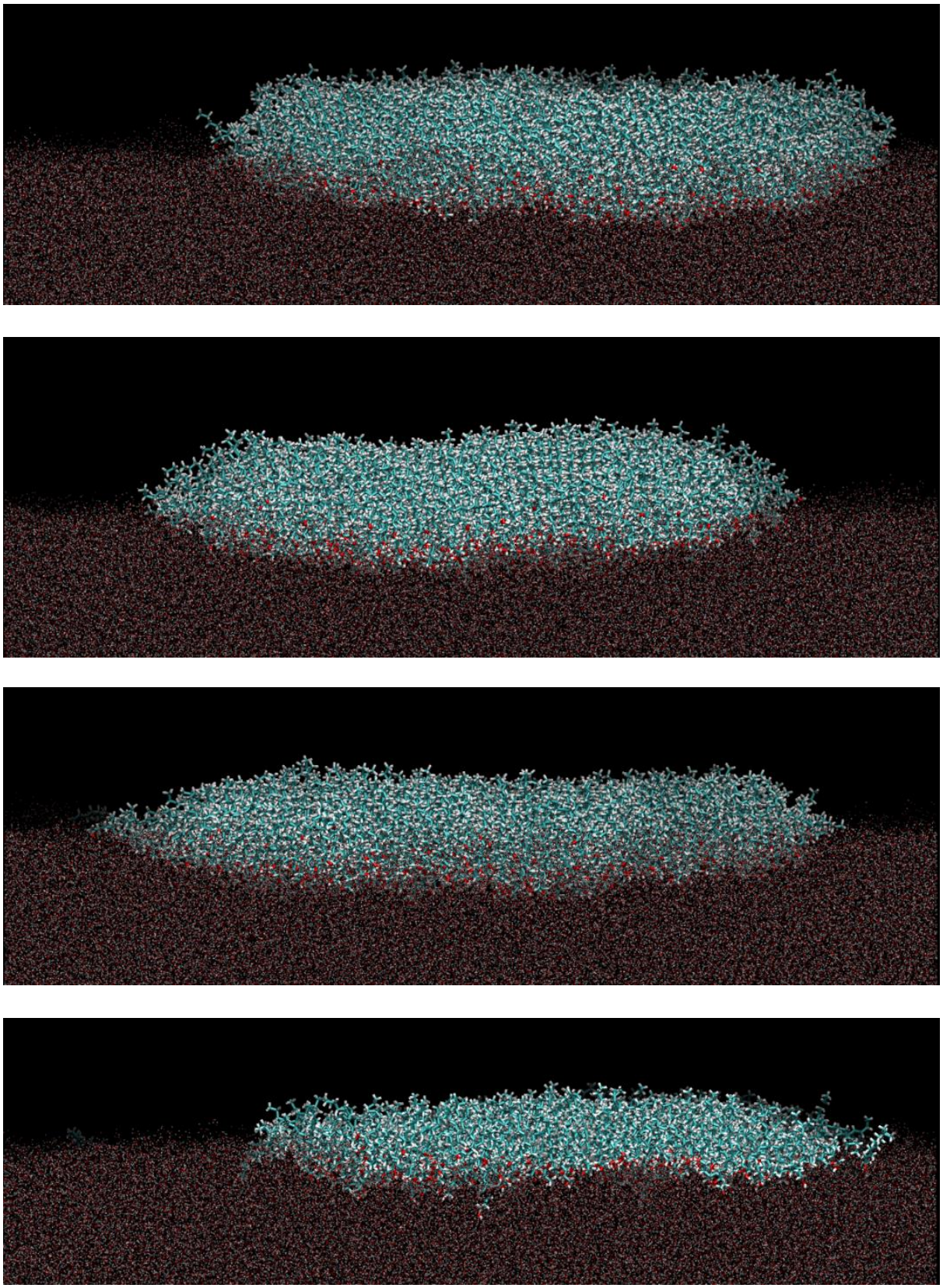

Figure 20 - Side view simulation snapshots of H18OH, H16OH, H14OH and H12OH systems (top to bottom), after 10 ns of simulation time. All boxes contain 550 amphiphile molecules at a molecular area of 0.6 nm^2/molecule (18.2 nm side box).

By analysis of Figure 17, it is clear that all shown fluorinated alcohol systems are organized on a 2D hexagonal packing structure since every inner molecule has 6 others surrounding it. Additionally, it is evident that the shorter the base molecule is, the less cohesive the system becomes. From both perspectives (Figure 17 and Figure 18) and from the visualization of the simulation trajectories, it can be seen that the number of laid down molecules on the periphery significantly increases from the F18OH through to the F12OH systems, as well as the frequency with which the molecules bend and tilt.

As for the hydrogenated alcohols (Figure 19 and Figure 20), there seems to be a local hexagonal lattice organization in the H18OH, H16OH and H14OH systems, which is quickly lost with distance. The molecules are more disorganized when compared to their fluorinated counterparts, culminating in what appears to be a layer of laid down molecules for the H12OH system.

4.3.2. Molecular Tilt Distribution

A study into the tilt angle of the systems of perfluorinated alcohols showed in the previous section was made. Intuitively, it can be said that the cohesion energy would increase with the increase of the fluorocarbon chain length, leading to a more stable, condensed and rigid film, resulting in a system more parallel to the z-axis.

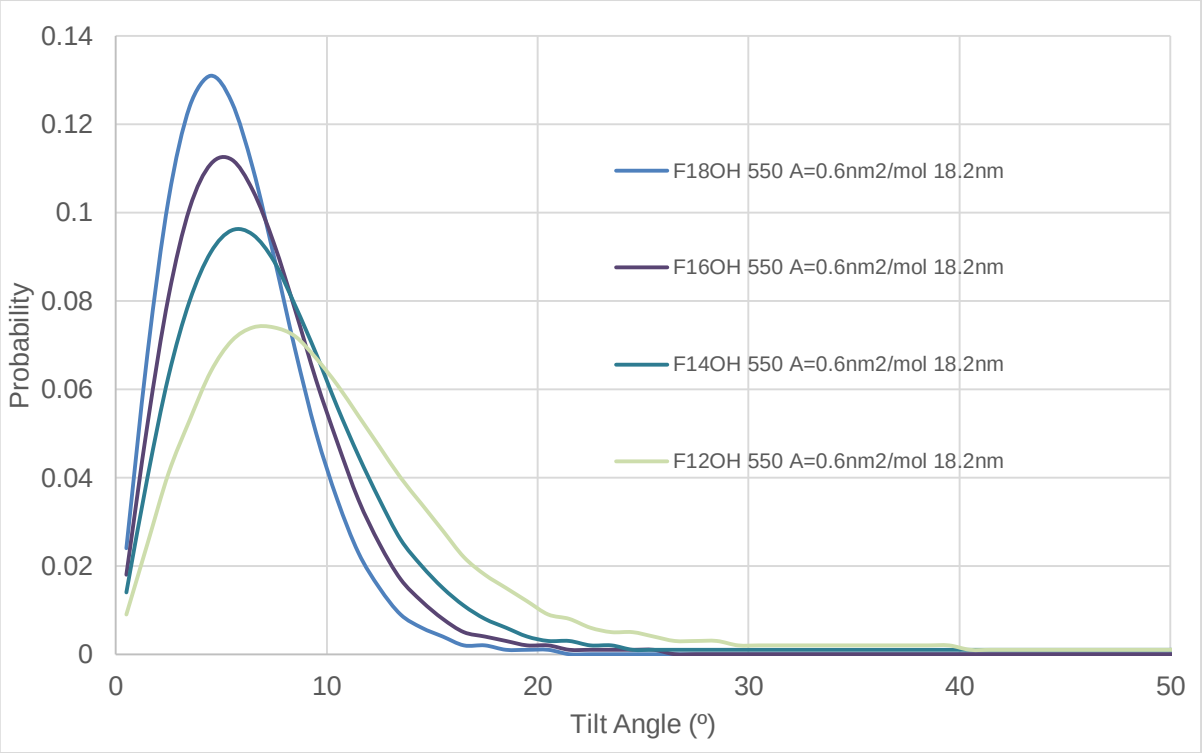

Figure 21 - Probability vs Tilt Angle for systems of perfluorinated alcohols with different chain lengths, in 18.2 nm side boxes.

As expected, the longer the base molecule is, the more tapered the bell curve becomes, meaning a decrease of the standard deviation. This implies that shorter chain molecules have more individual freedom of mobility. In addition, the average tilt angle value only changes very slightly, which indicates that the most upright molecules for the different films behave identically.

From the analysis of every system top view snapshots (Figure 17), it can be seen that the number of laid down molecules on the periphery of the monolayers increases significantly (as shown by the higher “tail” of the distribution), contributing to the increase of the average tilt angle. These units seem to affect the adjacent molecules to have a more flexible and less stiff behavior, which is progressively amplified the shorter the base molecule is.

4.3.3. Order Parameter

This study was also made for different chain length hydrogenated and perfluorinated alcohols. It was calculated by block averaging 8 ns of production time in 2 ns intervals with the exception of the H14OH system, for which only 4 ns of production time were used since it took more time to equilibrate. The obtained results are displayed in Figure 22.

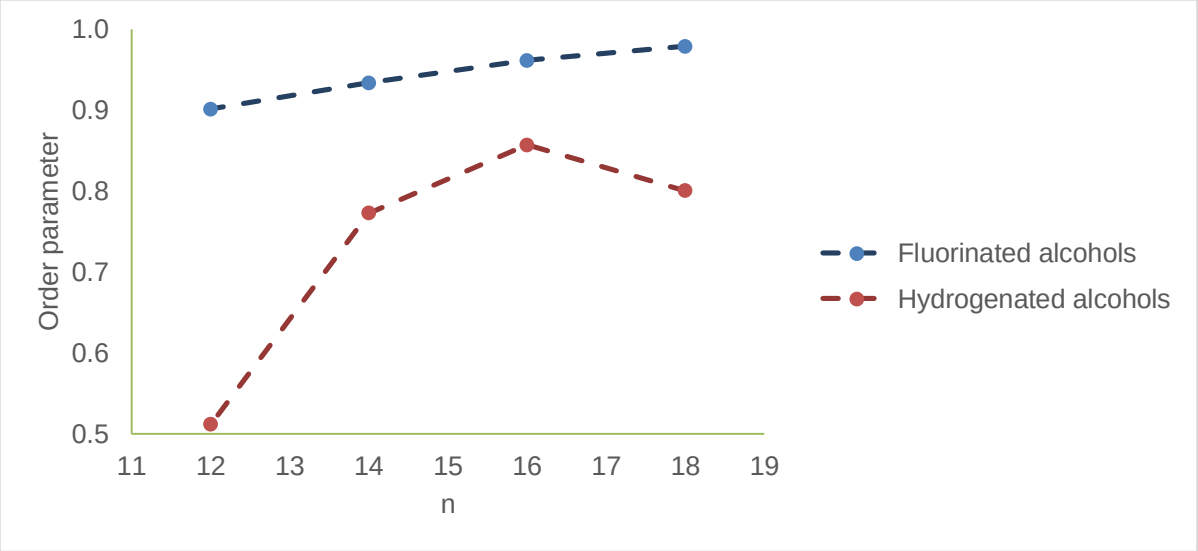

Figure 22 - Average Order Parameter (⟨OP⟩) vs n (number of carbon atoms in the molecule) for F18OH, F16OH, F14OH, F12OH systems and their hydrogenated homologues). All films contained 550 molecules at a molecular area of 0.6 nm^2/molecule.

As shown, all the simulated perfluorinated alcohol systems display ⟨OP⟩ values above 0.9, indicating a high propensity for the fluorocarbon chains to organize laterally, even for the shortest one, F12OH.

Additionally, it can be seen that a higher chain length results in a higher degree of parallelism since the values of ⟨OP⟩ steadily increase as a function of n. This stems from a higher structural stiffness in the inner parts of the films and the fact that there are fewer laid down molecules in the periphery. As predicted, the order parameter is significantly lower for their hydrogenated counterparts, particularly for dodecanol.

The highest discrepancy between consecutive compounds in this analysis is between H14OH and H12OH. This difference in order is very well portrayed in Figure 19 snapshots, in which is clear that while some of the H14OH molecules stand upright and a low degree of order can be seen, the H12OH seems to be a completely disordered liquid, where the vast majority of the molecules are laid down in a parallel plane to the water surface.

4.3.4. Dihedral Angle Distribution

The influence of the fluorocarbon chain length in dihedral angle distribution was also tested. The results for different chain length perfluorinated alcohols systems are presented below, in Figure 23 and Figure 24.

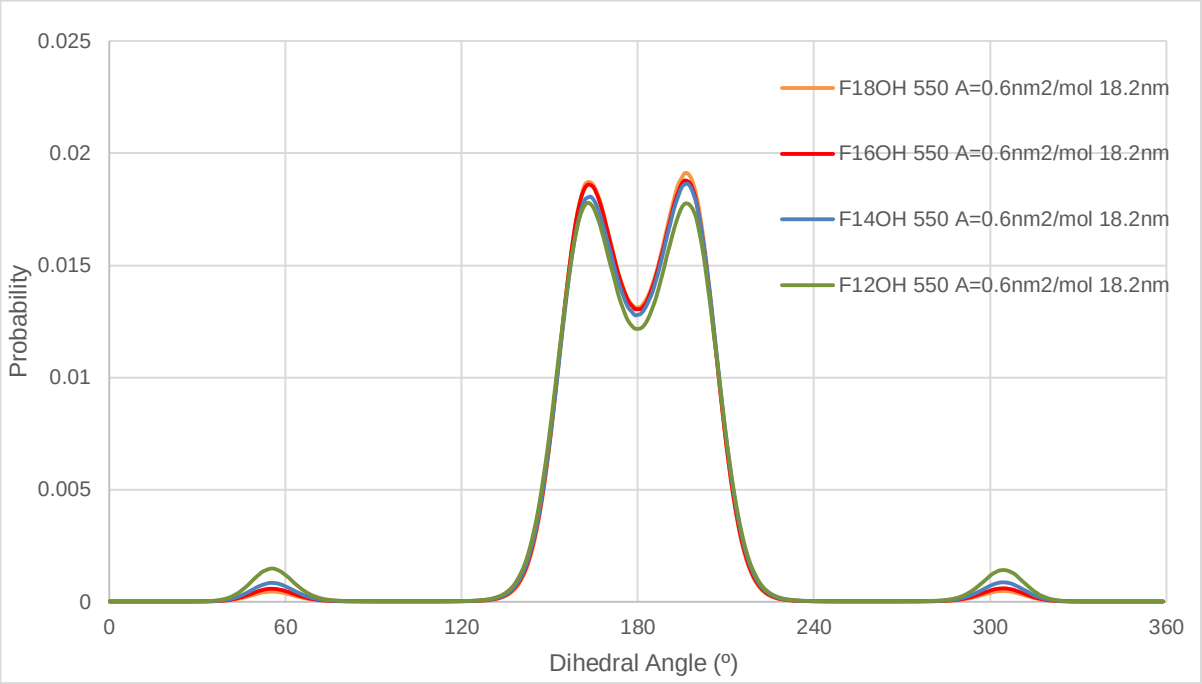

Figure 23 - Probability vs Dihedral Angle for systems comprised of 550 molecules of different chain length perfluorinated alcohols in 18.2 nm side boxes.

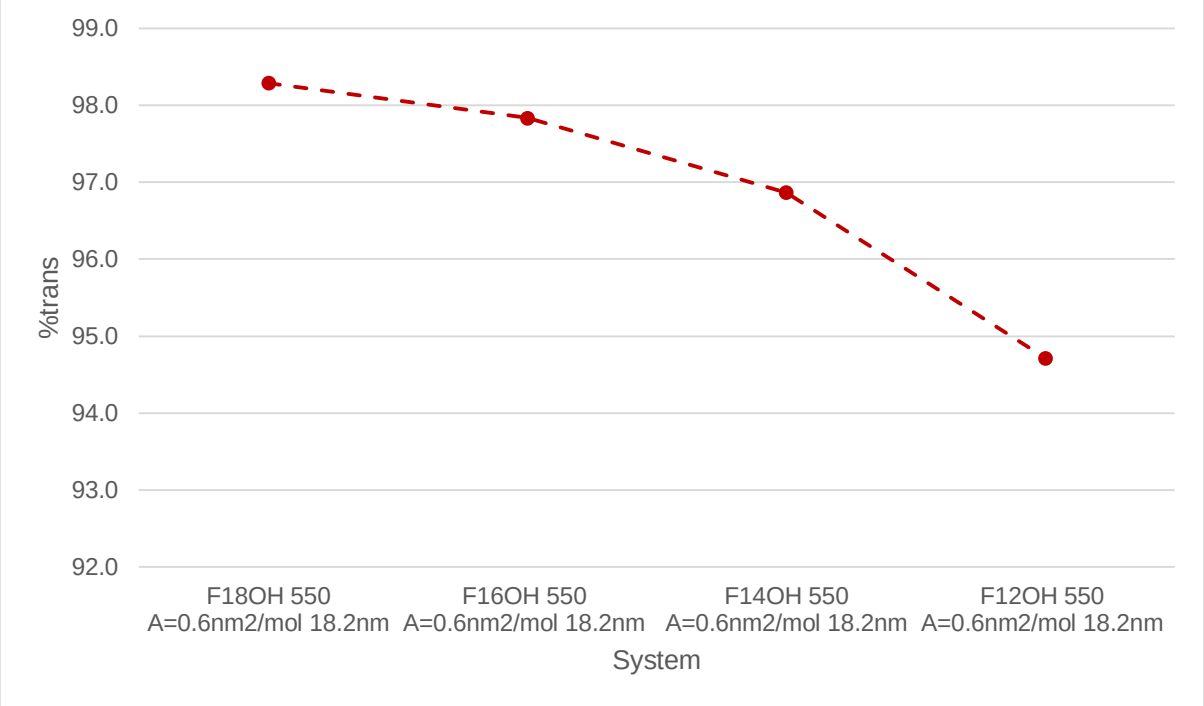

Figure 24 - *Trans* conformation probability density for the systems from Figure 23. *Gauche* and *trans* correspond to dihedral angle ranges of [0º,119º]∪[240º,359º] and [120º,239º], respectively.

In Figure 23, it is shown that *trans* conformations are significantly more likely to happen than *gauche* ones, although at distinct ratios, which are detailed in Figure 24. As depicted, the likelihood of *gauche* arrangements decreases with the increase of the chain length. This assessment, together with what was found in the Order Parameter section (4.3.3), makes it plausible to conclude that the suppression of *gauche* defects results in more rigid and cohesive domains. An overview also shows that none of the sides of the rotations is generally favored.

4.3.5. GIXD

In order to study quantitatively the structure of perfluorinated alcohol monolayers, full Grazing Incidence X-Ray Diffraction (GIXD) spectra were obtained for the simulated systems of F18OH, F16OH, F14OH and F12OH as well as for their hydrogenated equivalents. As previously mentioned in 2.1.1, simulated GIXD spectra can be obtained from the simulation trajectories [41]. The predicted GIXD spectra were calculated from 80 equally spaced simulation frames, at 100 ps intervals, covering 8 ns of production time. These results and the calculated lattice characterization parameters were then compared with experimental ones.

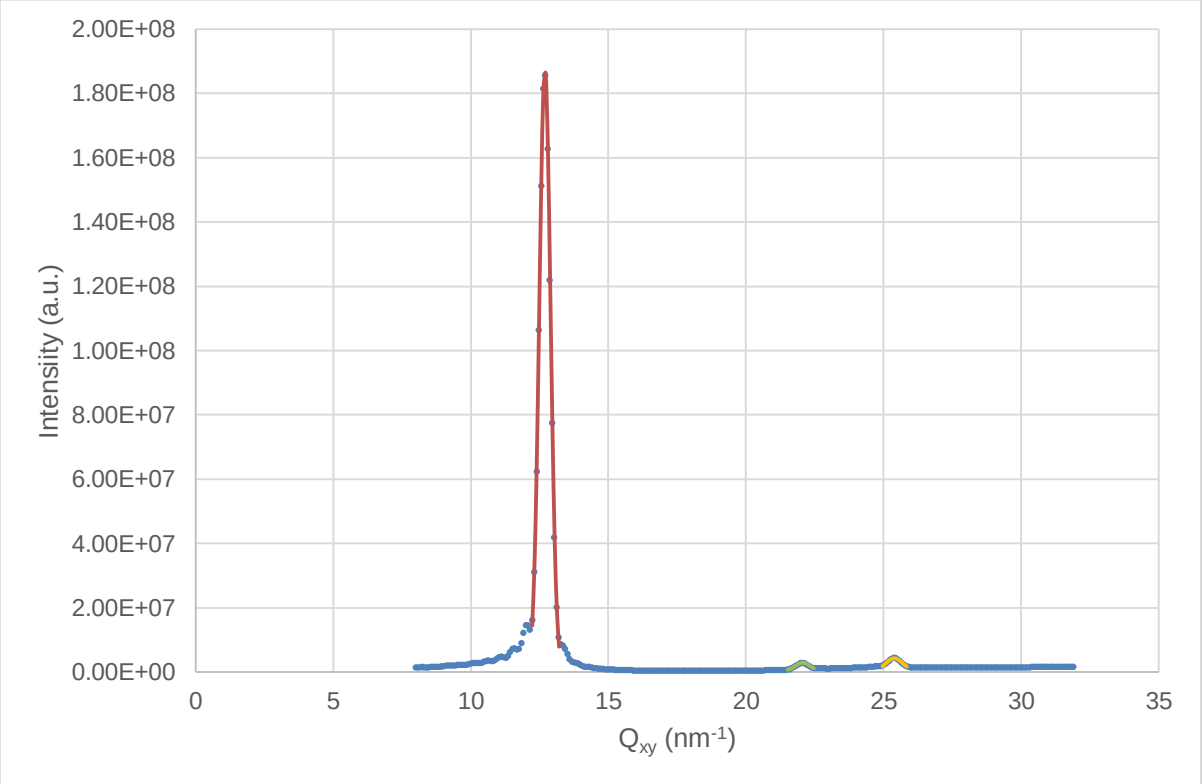

Figure 25 - Simulated diffraction spectra and Gaussian fits for the presented peaks for a system of 550 F18OH molecules at a molecular area of 0.6 nm^2/molecule (18.2 nm side box).

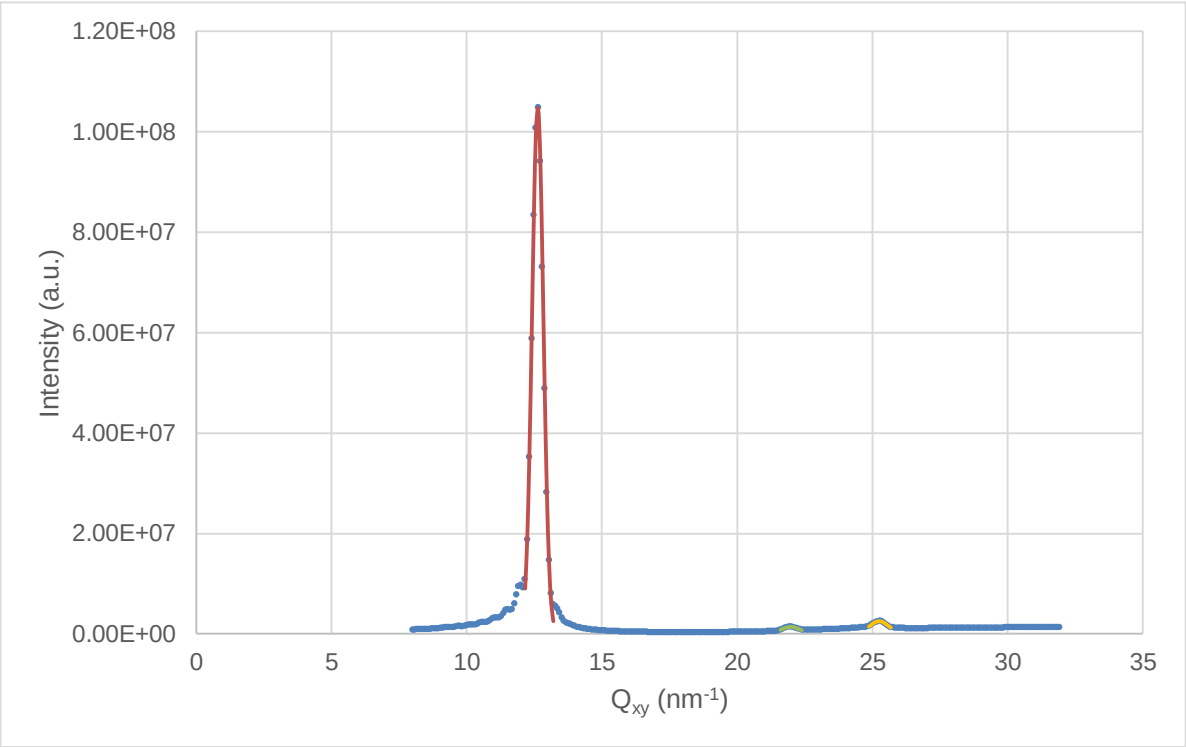

Figure 26 - Simulated diffraction spectra and Gaussian fits for the presented peaks for a system of 550 F16OH molecules at a molecular area of 0.6 nm^2/molecule (18.2 nm side box).

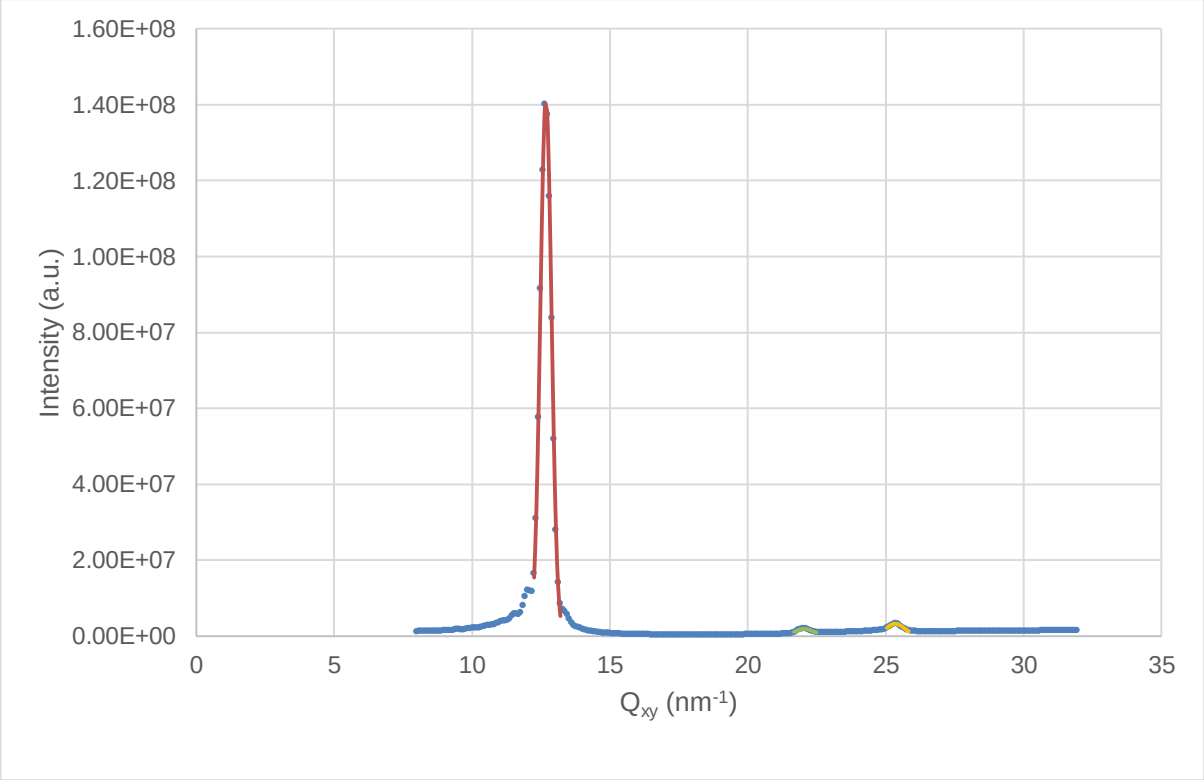

Figure 27 - Simulated diffraction spectra and Gaussian fits for the presented peaks for a system of 550 F14OH molecules at a molecular area of 0.6 nm^2/molecule (18.2 nm side box).

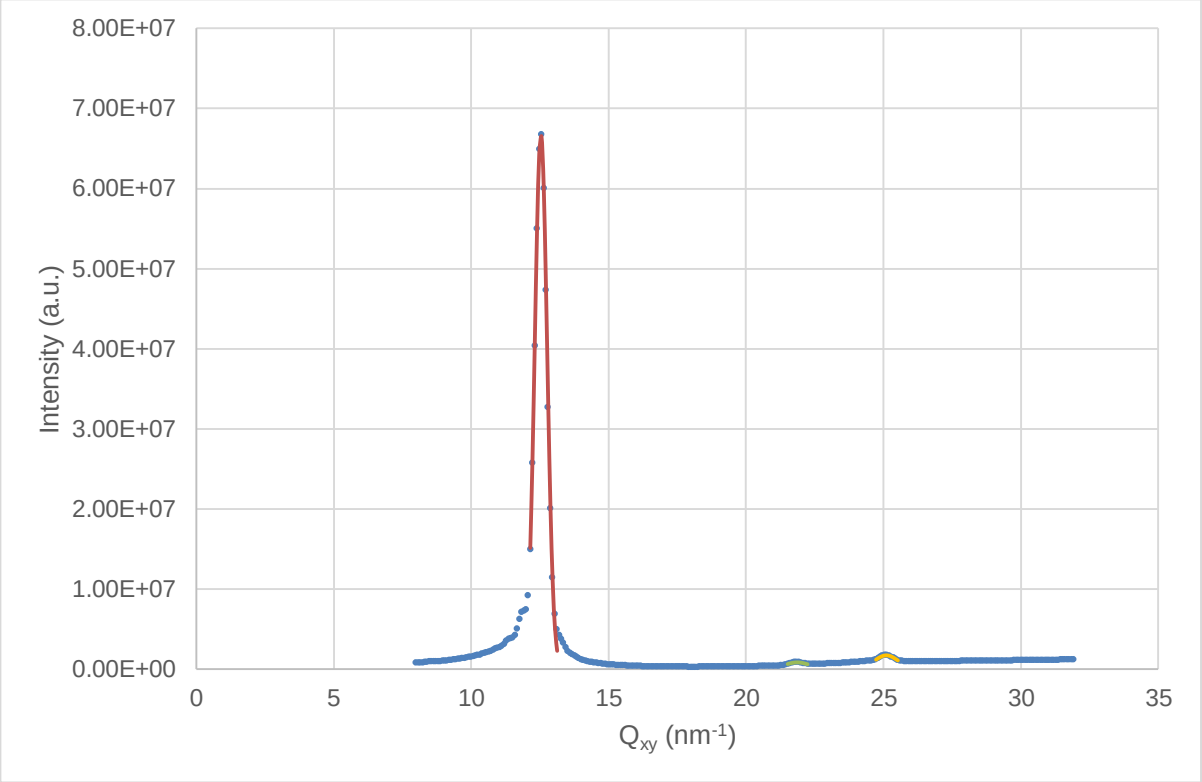

Figure 28 - Simulated diffraction spectra and Gaussian fits for the presented peaks for a system of 550 F12OH molecules at a molecular area of 0.6 nm^2/molecule (18.2 nm side box).

Within the studied limits of Q_{xy}, 3 peaks can be identified for the fluorinated alcohols data shown above in Figure 25-Figure 28: the lowest peak position with the highest intensity (attributed to Q_{10}) and 2 less intense peaks – attributed to Q_{11} and Q_{20}. If the lattice is hexagonal, the conditions $\frac{Q_{11}}{Q_{10}}=\sqrt{3}=1.732$ and $\frac{Q_{20}}{Q_{10}}=2$ should be met, which was verified for all the fluorinated molecules, as shown in Table 1.

Table 1 - Characteristics of the peaks from GIXD spectra for all fluorinated compounds in study for a system of 550 molecules at a molecular area of 0.6 nm^2/molecule (18.2 nm side box).

	Base molecule			
Peak	**F18OH**	**F16OH**	**F14OH**	**F12OH**
Q_{10} (nm^{-1})	12.69	12.67	12.62	12.54
Q_{11} (nm^{-1})	22.07	22.05	21.98	21.86
Q_{20} (nm^{-1})	25.39	25.35	25.25	25.10
$\frac{Q_{11}}{Q_{10}}$	1.738	1.740	1.741	1.744
$\frac{Q_{20}}{Q_{10}}$	2.000	2.000	2.001	2.001

Table 2 - Structural parameters for different chain length perfluorinated alcohols for simulated systems of 550 molecules at a molecular area of 0.6 nm^2/molecule (18.2 nm side box).

	Base molecule			
Property	**F18OH**	**F16OH**	**F14OH**	**F12OH**
Q_{10} (nm^{-1})	12.69	12.67	12.62	12.54
$\langle d_{10} \rangle$ (nm)	0.5715	0.5726	0.5747	0.5786
$\langle A \rangle$ (nm^2/molecule)	0.2829	0.2839	0.2861	0.2899

Using the Gaussian fit of the GIXD spectra data, the different systems can be characterized through different parameters, shown in Table 2. As exhibited, it can be seen that as the chain length decreases, the hexagonal lattice parameter, $\langle d_{10} \rangle$, and, consequently, the average effective molecular area, $\langle A \rangle$, both increase. This is because the fewer atoms the carbon chain backbone has, the weaker intermolecular forces are. Therefore, there is more available space between them, reducing rigidity and stiffness and making the system more fluid and less cohesive.

Moreover, these results can be compared with experimental GIXD results for the F18OH and F14OH, shown in [53]. Experimental GIXD spectrum of a F18OH system at a surface pressure of 15 mN/m is represented in Figure 29 and its characterization is in Table 3. In addition, Figure 30 depicts experimental GIXD spectrum of a F18OH system located in the near-zero surface pressure plateau, which was used for comparison with simulated GIXD data. This differentiation is detailed in Table 4.

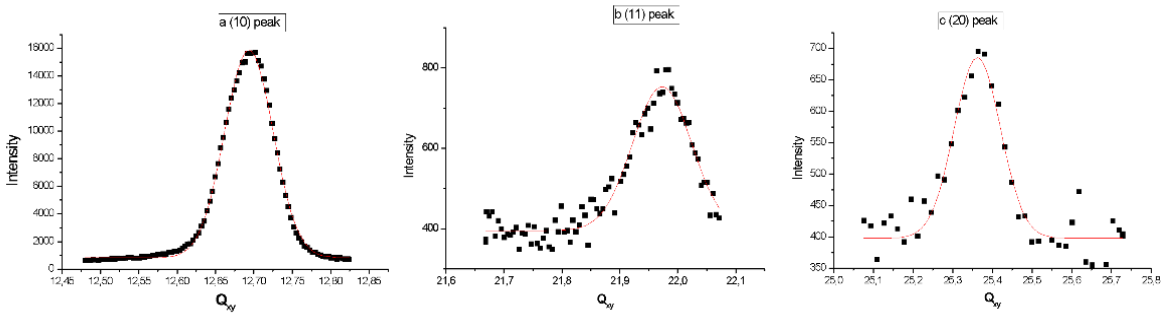

Figure 29 – Experimental Q_z integrated diffraction spectrum at 18°C and 15 mN/m of the F18OH Langmuir film. a) Q_{10} peak; b) Q_{11} peak; c) Q_{20} peak. Adapted from [53].

Table 3 - Positions of the F18OH diffraction peaks at 15 mN/m obtained by Gaussian curve fitting. Data from [53].

Peak	Peak position (nm^{-1})
Q_{10} (nm^{-1})	12.69
Q_{11} (nm^{-1})	21.97
Q_{20} (nm^{-1})	25.36
$\frac{Q_{11}}{Q_{10}}$	1.731
$\frac{Q_{20}}{Q_{10}}$	2.000

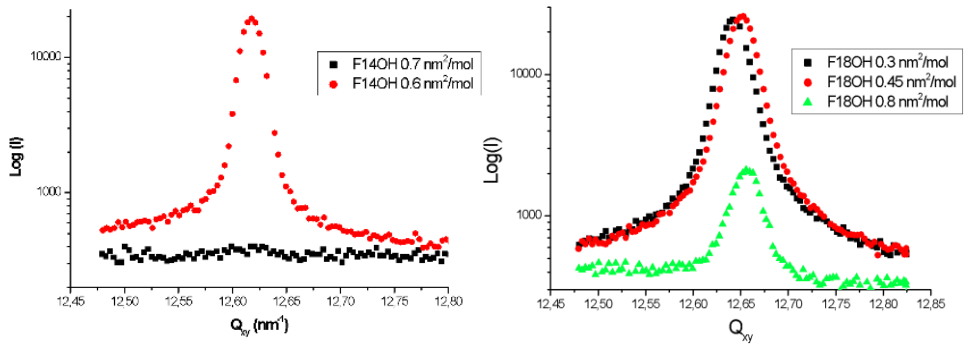

Figure 30 – Experimental diffraction spectra at 18°C of the Langmuir films of F14OH (left) and F18OH (right) at different molecular areas along the near-zero surface pressure plateau. Figure adapted from [53].

Table 4 - Comparison of GIXD relevant parameters for experimental results of F18OH at a molecular area of 0.45 nm^2/molecule and F14OH at a molecular area of 0.6 nm^2/molecule, at 18ºC (Figure 30), versus simulation results of F18OH and F14OH of systems with 550 molecules, both at 20ºC and molecular areas of 0.6 nm^2/molecule. Experimental data from [53].

Parameter	Base molecule	Experimental	Simulated
Q_{10} (nm^{-1})	F18OH	12.65	12.69
	F14OH	12.62	12.62
⟨A⟩ (nm^2/molecule)	F18OH	0.285	0.283
	F14OH	0.286	0.286
Coherence length (nm)	F18OH	300	13.4
	F14OH	>320	12.8

Since the difficulty to obtain meaningful signals in GIXD for Langmuir films increases with the decrease of surface pressure, the lower the molecular density is in a specific system, the less distinguishable the diffraction peaks are, which is significant for the minor peaks for the cases in study - Q_{11} and Q_{20}. For this reason, [53] shows 3 viable peaks for the system at 15 mN/m (Figure 29), but only Q_{10} could be found at near-zero surface pressure (Figure 30). However, the ratios of the positions of the peaks for the former, shown in Table 3, are in agreement with the hexagonal lattice, and since the position of the major peak (Q_{10}) is identical in both cases (12.69 nm^{-1} vs 12.65 nm^{-1}), it is reasonable to assume that the crystalline organization does not change significantly from 15 mN/m to zero surface pressure, which is the case for the molecular area of 0.6 nm^2/molecule of the simulated systems used for comparison.

Table 4 shows that both the prominent peak's position and the limit molecular area values are very similar between experimental the GIXD results and the GIXD spectra obtained from MD simulations. On the contrary, the coherence length parameter shows high disparity, which is explained by the simulation method's limitations. The values shown experimentally, in the order of hundreds of nanometers, are not reproducible since it would require much larger boxes with a much higher number of water and F18OH/F14OH molecules, which is computationally unfeasible. Thus, the values obtained for this parameter for the simulated systems are limited by the aggregate's diameter, which is approximately 14.2 nm and 14.4 nm for the F18OH and F14OH systems, respectively. Nevertheless, the overall results show an almost perfect accordance between simulated and experimental results, supporting the hypothesis that the simulations represent these monolayers real structure at a molecular level.

Furthermore, the AFM results from literature presented previously (Figure 6 - 3. State of the Art) support these findings. Both F14OH and F18OH systems were shown to arrange themselves in a hexagonal lattice, although AFM results show a significant difference in the detail relative to regular hexagonal figures. The F14OH system is mainly made of filament-like structures than detailed hexagonal structures, which contrasts with the F18OH system. The higher number of laid down

molecules in the F14OH system (Figure 17) may help explain why the limits of the aggregates are less well defined than in the F18OH images. In both alcohols, the visible domains height profile is identical to the length of the fully extended molecules, suggesting that these compounds are perpendicular to the water substrate within the aggregates, which is also consistent with experimental GIXD results [53].

The GIXD spectra of the hydrogenated alcohols was also calculated. They showed a single peak broader and of higher order than that of the Q_{10} ones obtained for the fluorinated alcohols (Appendix C). This shows that despite a signal that reflects systematic organization is detected, the coherence length is very short and the observed order is only local. This might be the reason why it is not observed in an experimental and macroscopic scale.

5. Conclusion

Motivated by the different behavior between hydrogenated alcohols and perfluorinated ones, several molecular dynamics simulations of monolayers containing units of these groups were conducted in order to characterize their structure and behavior at a molecular scale.

A Gas phase was first observed for the system of 5 molecules in an 18.2 nm side box, at a molecular area of 66.2 nm^2/molecule. Some of the molecules were found to disassemble from the tight cylindrical initial configuration and spent a significant amount of simulation time moving freely throughout the water surface, while occasionally returning to a centered aggregate.

As could be predicted, the aggregate's size was found to be very significant in the behavior of the Langmuir films. Molecules in very small aggregates were determined to be almost parallel to the water surface and disordered, and the increase of the number of molecules in the monolayer resulted in more ordered domains and closer to being parallel to the z-axis. A correlation between the degree of order and atomic spatial configurations was also detected, since bigger aggregates showed a higher tendency to suppress *gauche* defects.

The influence of the chain length of the base molecule was studied for systems of perfluorinated and hydrogenated alcohols at a molecular area located in the coexistence plateau. A preliminary snapshot analysis of these systems showed a loss of organization with the shortening of the carbon chain, albeit more significant for the hydrogenated compounds. For the first, the molecular tilt distribution confirmed this, as it showed a higher freedom of molecular mobility for the shorter perfluorinated alcohols.

The order parameter analysis showed a steady increase for the perfluorinated alcohols with the number of chain carbons and a non-monotonous variation (but an overall increase) for the hydrogenated alcohols. It was most impressive to note that the average order parameter of the shortest fluorocarbon system (F12OH) was higher than that of the longest hydrogenated alcohol system (H18OH), reflecting the higher stiffness and intermolecular cohesion associated with fluorinated chains.

Dihedral angle distributions showed that *trans* conformations are always highly favored over *gauche* conformations independently of the size of the perfluorinated molecule in question, although the latter being more suppressed the longer the base molecule is.

Finally, it was determined from simulated GIXD spectra that every perfluorinated alcohol Langmuir film follows a hexagonal lattice structure. Also, the calculated parameters for this method showed to be in very good agreement with experimental data. This is, in all likelihood, the most important finding of this work, as it validates the foundation of the studies made – the used force field.

In summary, the results presented in this work proved the intrinsic ability of perfluorinated molecules to aggregate in highly organized 2D hexagonal structures, even at high molecular areas and for short chain compounds, which become more cohesive and stable with the increase of both the size of the molecule and the aggregate.

5.1. Future Work

Further investigation work must be made to better understand the structure and behavior of perfluorinated alcohols. Including:

- Experimental isotherm studies at different temperatures for different amphiphilic molecules.

- Molecular dynamics simulations for amphiphiles with different head groups. Additionally, for perfluorinated alcohols evaluate the effects of the number of H-spacers.

- Molecular dynamics simulations of systems with equal molecular areas but different aggregate sizes.

- Simulate bigger aggregates in larger boxes, to reduce the error in quantitative measurements as well as the influence of the periodic boundary conditions.

6. References

[1] P. J. Denning and T. G. Lewis, "Exponential Laws of Computing Growth," *Communications of the ACM,* vol. 60, no. 1, pp. 54-65, 2017.

[2] E. Kissa, "Fluorinated surfactants, synthesis, properties, applications," in *Surfactant Science Series*, New York, Marcel Dekker, 1994.

[3] M. P. Krafft, "Fluorocarbons and fluorinated amphiphiles in drug delivery andbiomedical research," *Advanced Drug Delivery Reviews,* vol. 47, no. 2-3, pp. 209-228, 2001.

[4] J. G. Riess, "Perfluorochemical emulsions for intravascularuse: principles, materials and methods," in *Fluorine in Medicine in the 21st Century*, University of Manchester, 1994, pp. 1-9.

[5] H. Nakahara, S. Nakamura, H. Kawasaki and O. Shibata, "Properties of two-component Langmuir monolayer of single chain perfluorinated carboxylic acids with dipalmitoylphosphatidylcholine," *Colloids and Surfaces B: Biointerfaces,* vol. 41, no. 4, p. 285–298, 2005.

[6] A. Bondi, "Van der Waals volumes and radii," *The Journal of Physical Chemistry ,* vol. 68, no. 3, pp. 441-451, 1964.

[7] G. J. T. Tiddy, "Concentrated surfactant systems," in *H.F. Eicke (Ed) Modern Trends of Colloid Science in Chemistry and Biology*, Basel, Birkhauser Verlag, 1985, pp. 148-159.

[8] M. J. Rosen, Surfactants and Interfacial Phenomena, New York: Wiley, 1978.

[9] H. Hoffmann, J. Kalus and H. Thurn, "Small angle neutron scattering measurements on micellar solutions of perfluor detergents," *Colloid and Polymer Science,* no. 261, p. 1043–1049, 1983.

[10] D. F. Eaton and B. E. Smart, "Are fluorocarbon chains ‘stiffer’ than hydrocarbon chains? Dynamics of end-to-end cyclization in a C8F16 segment monitored by fluorescence," *Journal of the American Chemical Society,* no. 112, p. 2821–2823, 1990.

[11] D. W. R. Gruen, "A model for the chains in amphiphilic aggregates. 2. Thermodynamic and experimental comparisons for aggregates of different shape and size," *The Journal of Physical Chemistry,* no. 89, p. 153–163, 1985.

[12] P. J. Flory, Statistical Mechanics of Chain Molecules, New York: Interscience Publications, 1969.

[13] H. A. Rigby and C. W. Bunn, " A room-temperature transition in polytetrafluoroethylene," *Nature,* no. 164, p. 583–585, 1949.

[14] G. T. Furukawa, R. E. McCoskey and G. J. King, " Calorimetric properties of polytetrafluoroethylene (Teflon)," *Journal of research of the National Bureau of Standards,* no. 49, p. 273, 1952.

[15] M. P. Krafft and M. Goldmann, "Monolayers made from fluorinated amphiphiles," *Current Opinion in Colloid and Interface Science,* vol. 8, no. 3, pp. 243-250, 2003.

[16] T. Takiue and D. Vollhardt, "Miscibility of alkanol and fluoroalkanol in Langmuir film at the airywater interface," *Colloids and Surfaces,* pp. 198-200; 797-804, 2002.

[17] J. G. Reiss and P. E. Keipert, "Update on perfluorocarbon-based oxygen delivery systems," in *Blood Substitutes — Present and Future Perspectives*, Amsterdam, Elsevier, 1998, pp. 91-101.

[18] J. G. Riess, "Highly fluorinated systems for oxygen transport, diagnosis and drug delivery," *Colloids and Surfaces A: Physicochemical and Engineering Aspects,* vol. 84, no. 1, pp. 33-48, 1994.

[19] P. Morgado, J. B. Lewis, C. M. Laginhas, L. F. Martins, C. McCabe, F. J. Blas and E. J. Filipe, "Systems involving hydrogenated and fluorinated chains: Volumetric properties of perfluoroalkanes and perfluoroalkylalkane surfactants," *Journal of Physical Chemistry B,* vol. 115, no. 50, pp. 15013-15023, 2011.

[20] M. P. Krafft and J. G. Riess, "Perfluorocarbons: Life Sciences and Biomedical Uses," *Journal of Polymer Science Part A: Polymer Chemistry,* vol. 45, pp. 1185-1198, 2006.

[21] J. G. Riess and M. L. Blanc, "Solubility and transport phenomena in perfluorochemicals relevant to blood substitution and other biomedical applications," *Pure and Applied Chemistry,* vol. 54, no. 12, pp. 2383-2406, 1982.

[22] J. G. Riess, "Fluorous micro- and nanophases with a biomedical perspective," *Tetrahedron,* vol. 58, no. 20, pp. 4113-4131, 2002.

[23] H. IT and J. Rabai, "Facile Catalyst Separation Without Water: Fluorous Biphase Hydroformylation of Olefins," *Science,* vol. 266, no. 5182, pp. 72-75, 1994.

[24] R. D. Chambers, Flourine in organic chemistry, Durham : Blackwell Publishing, 2004.

[25] D. M. Lemal, "Perspective on Fluorocarbon Chemistry," *Journal of Organic Chemistry,* vol. 69, no. 1, pp. 1-11, 2004.

[26] A. L. S. Gamboa, "Ordering in Langmuir and Langmuir-Blodgett films: effect of the presence of fluorocarbon and hydrocarbon chains," 2006.

[27] V. M. Kaganer, H. Mohwald and P. Dutta, "Structure and phase transitions in Langmuir monolayers," *Reviews of Modern Physics,* vol. 71, no. 3, pp. 779-819, 1999.

[28] M. Losche, E. Sackmann and H. Mohwald, "A Fluorescence Microscopic Study Concerning the Phase Diagram of Phospholipids," *Berichte Der Bunsen-Gesellschaft-Physical Chemistry Chemical Physics,* vol. 87, no. 10, pp. 848-852, 1983.

[29] V. M. Kaganer, M. A. Osipov and I. R. Peterson, "A molecular model for tilting phase transitions between condensed phases," *Journal Of Chemical Physics,* vol. 98, no. 4, pp. 3512-3527, 1993.

[30] W. L. Jorgensen, D. S. Maxwell and J. Tirado-Rives, "Development and testing of the OPLS all-atom force field on conformational energetics and properties of organic liquids," *Journal of the American Chemical Society,* vol. 118, no. 45, pp. 11225-11236, 1996.

[31] M. P. Allen, "Introduction to Molecular Dynamics Simulation," *Computational Soft Matter: From Synthetic Polymers to Proteins,* vol. 23, pp. 1-28, 2004.

[32] "GROMACS 2019 - Reference Manual - Interaction function and force fields," [Online]. Available: https://manual.gromacs.org/documentation/2019/reference-manual/functions/bonded-interactions.html. [Accessed 20 January 2021].

[33] E. Generalic, "Lennard-Jones potential," 20 October 2018. [Online]. Available: https://glossary.periodni.com/glossary.php?en=Lennard-Jones+potential. [Accessed 8 December 2020].

[34] "About GROMACS," 24 September 2018. [Online]. Available: http://www.gromacs.org/About_Gromacs. [Accessed 26 November 2020].

[35] S. Pronk, S. Pall, R. Schulz, P. Larsson, P. Bjelkmar, R. Apostolov, M. R. Shirts, J. C. Smith, P. M. Kasson, D. V. D. Spoel, B. Hess and E. Lindahl, "GROMACS 4.5: A high-throughput and highly parallel open source molecular simulation toolkit," *Bioinformatics,* vol. 29, no. 7, pp. 845-854, 2013.

[36] D. V. D. Spoel, E. Lindahl, B. Hess, G. Groenhof, A. E. Mark and H. J. Berendsen, "GROMACS: Fast, flexible, and free," *Journal of Computational Chemistry,* vol. 26, no. 16, pp. 1701-1718, 2005.

[37] L. Martínez, R. Andrade, E. G. Birgin and J. M. Martínez, "Packmol: A Package for Building Initial Configurations for Molecular Dynamics Simulations," *Journal of Computational Chemistry,* vol. 30, no. 13, pp. 2157-2164, 2010.

[38] "PACKMOL Initial configurations for Molecular Dynamics Simulations by packing optimization," [Online]. Available: http://m3g.iqm.unicamp.br/packmol/home.shtml. [Accessed 27 November 2020].

[39] "VMD," Theoretical and Computational Biophysics Group, 24 November 2020. [Online]. Available: https://www.ks.uiuc.edu/Research/vmd/. [Accessed 26 November 2020].

[40] W. Humphrey, A. Dalke and K. Schulten, "VMD: Visual Molecular Dynamics," *Journal of Molecular Graphics & Modelling,* vol. 14, no. 1, pp. 33-38, 1996.

[41] P. A. C. Lourenço, "Molecular Dynamics Simulations and Simulated Diffraction Spectra of Long Chain Fluorinated and Hydrogenated Substances at the Water-Air Interface," 2018.

[42] "Microsoft Office Excel," [Online]. Available: https://www.microsoft.com/pt-pt/microsoft-365/p/excel/cfq7ttc0k7dx?activetab=pivot%3aoverviewtab. [Accessed 27 November 2020].

[43] B. Hess, "P-LINCS: A Parallel Linear Constraint Solver for Molecular Simulation," *Journal of Chemical Theory and Computation,* vol. 4, no. 1, pp. 116-122, 2008.

[44] G. Bussi, D. Donadio and M. Parrinello, "Canonical sampling through velocity rescaling," *Journal of Chemical Physics,* vol. 126, no. 1, 2007.

[45] E. Duffy, "Ph.D. Thesis," New Haven, CT, USA, 1994.

[46] R. Chitra and P. Smith, "A comparison of the properties of 2,2,2-trifluoroethanol and 2,2,2-trifluoroethanol/water mixtures using different force fields," *The Journal of Chemical Physics,* vol. 115, no. 12, pp. 5521-5530, 2001.

[47] E. K. Watkins and W. L. Jorgensen, "Perfluoroalkanes: Conformational Analysis and Liquid-State Properties from ab Initio and Monte Carlo Calculations," *Journal of Physical Chemistry A,* vol. 105, no. 16, pp. 4118-4125, 2001.

[48] P. Fontaine, E. Filipe, M.-C. Fauré, T. Rego, S. Taßler, A. Alves, G. Silva, P. Morgado and M. Goldmann, "Structure of Langmuir Monolayers of Perfluorinated Fatty Acids: Evidence of a New 2D Smectic C Phase," *Molecules,* vol. 24, no. 19, p. 3590, 2019.

[49] K. Pluhackova, H. Morhenn, L. Lautner, W. Lohstroh, K. S. Nemkovski, T. Unruh and R. A. Bock-mann, "Extension of the LOPLS-AA Force Field for Alcohols, Esters, and Monoolein Bilayers and its Validation by Neutron Scattering Experiments," *Journal of Physical Chemistry B,* vol. 119, no. 49, pp. 15287-15299, 2015.

[50] H. J. Berendsen, J. R. Grigera and T. P. Straatsma, "The missing term in effective pair potentials," *Journal of Physical Chemistry,* vol. 91, no. 24, pp. 6269-6271, 1987.

[51] V. Vins, D. Celný, B. Planková, T. Nemec, M. Duska and J. Hrubý, "Molecular Simulations of the Vapor–Liquid Phase Interfaces of Pure Water Modeled with the SPC/E and the TIP4P/2005 Molecular Models," *EPJ Web of Conferences,* vol. 114, 2016.

[52] S. W. Barton, A. Goudot, F. R. Othman Bouloussa, B. Lin, F. Novak, A. Acero and S. A. Rice, "Structural transitions in a monolayer of fluorinated amphiphile molecules," *The Journal of Chemical Physics,* vol. 96, no. 2, p. 1343, 1992.

[53] P. Silva, D. Nova, M. Teixeira, V. Cardoso, P. Morgado, B. Nunes, R. Colaço, M.-C. Fauré, P. Fontaine, M. Goldmann and E. J. M. Filipe, "Langmuir Films of Perfluorinated Fatty Alcohols: Evidence of Spontaneous Formation of Solid Aggregates at Zero Surface Pressure and Very Low Surface Density," *Nanomaterials,* vol. 10, no. 11, p. 2257, 2020.

[54] M. Rusdi, Y. Moroi, S. Nakamura, O. Shibata, Y. Abe and T. Takahashi, "Mixed Langmuir Monolayer of N-(1,1-Dihydroperfluorododecyl)-N,N,N-Trimethylammonium Chloride with Perfluorocarboxylic Acids," *Journal of Colloid and Interface Science,* vol. 243, no. 2, pp. 370-381, 2001.

[55] B.-Y. Zhu, P. Zhang, R.-X. Wang, Z.-F. Liub and L.-H. Lai, "Phase separation and crystallization in mixed monolayers of FC and HC surfactants," *Colloids and Surfaces A: Physicochemical and Engineering Aspects,* vol. 157, no. 1-3, pp. 63-71, 1999.

[56] M. C. Teixeira, "Complex Interfacial Behaviour of Mixtures of Fluorinated and Hydrogenated Alcohols," 2014.

Appendix A

Table 5 - Non-bonded parameters of the force-fields used in the simulations.

Site	σ (nm)	ε (kJ/mol)	Q (e)	Designation
FnOH				
C (CF_3)	0.350	0.276144	+0.450	C_F
C (CF_2CH_2OH, perfluorinated)	0.325	0.259408	+0.430	
C (CF_2, all other cases)	0.350	0.276144	+0.300	
C (CH_2OH)	0.350	0.276144	+0.126	C_{OH}
F (CF_3,CF_2)	0.295	0.221752	-0.150	F
F (CF_2CH_2OH)	0.294	0.239911	-0.258	
H (CH_2)	0.250	0.125520	+0.083	H_C
H (OH)	0	0	+0.429	H_O
O (OH)	0.307	0.711280	-0.635	O
H_2O				
O	0.316557	0.650194	-0.8476	O
H	0	0	+0.4238	H
HnOH				
C (CH_3)	0.350	0.276144	-0.222	C_H
C (CH_2)	0.350	0.276144	-0.148	
C (CH_2OH)	0.350	0.276144	+0.145	C_{OH}
H (CH_3)	0.250	0.125520	+0.074	H
H (CH_2)	0.250	0.110000	+0.074	
H (CH_2OH, methylene)	0.250	0.125520	+0.060	$H_{CH2OH,methylene}$
H (CH_2OH, alcohol)	0	0	+0.418	H_O
O (OH)	0.312	0.711280	-0.683	O

Table 6 - Bond stretching parameters used in the simulations. Atoms are designated as shown in Table 5.

Bond	r_{eq} **(nm)**	k_{ij}^{r} **(kJ/(mol.nm^2))**
FnOH		
C_F-F	0.13320	307105.6
C_F-C_F	0.15290	224262.4
C_{OH}-C_F	0.15290	224262.4
C_{OH}-H_C	0.10900	284512.0
C_{OH}-O	0.14100	267776.0
O-H_O	0.09450	462750.4
H_2O (rigid)		
	r **(nm)**	
O-H	0.1	
HnOH		
C_H-C_H	0.15290	224262.4
C_H-C_{OH}	0.15290	224262.4
C_H-H	0.10900	284512.0
C_{OH}-$H_{CH2OH,methylene}$	0.10900	284512.0
C_{OH}-O	0.14100	267776.0
O-H_O	0.09450	462750.4

Table 7 - Bond angle parameters used in the simulations. Atoms are designated as shown in Table 5.

Angle	θ_{eq} (º)	k_{ijk}^{θ} (kJ/(mol.rad^2))
FnOH		
F-C_F-F	109.10	644.336
F-C_F-C_F	109.50	418.400
C_F-C_F-C_F	112.70	488.273
C_F-C_F-C_{OH}	112.70	488.273
F-C_F-C_{OH}	109.50	418.400
C_F-C_{OH}-H_C	110.70	313.800
C_F-C_{OH}-O	109.50	418.400
H_C-C_{OH}-H_C	107.80	276.144
H_C-C_{OH}-O	109.50	292.880
C_{OH}-O-H_O	108.50	460.240
H_2O (rigid)		
	θ (º)	
H-O-H	109.47	
HnOH		
H-C_H-H	107.80	276.144
H-C_H-C_H	110.70	313.800
C_H-C_H-C_H	112.70	488.273
C_H-C_H-C_{OH}	112.70	488.273
H-C_H-C_{OH}	110.70	313.800
C_H-C_{OH}-$H_{CH2OH,methylene}$	110.70	313.800
C_H-C_{OH}-O	109.50	418.400
$H_{CH2OH,methylene}$-C_{OH}-$H_{CH2OH,methylene}$	107.80	276.144
$H_{CH2OH,methylene}$-C_{OH}-O	109.50	292.880
C_{OH}-O-H_O	108.50	460.240

Table 8 - Dihedral parameters used in simulations (Ryckaert-Bellemans type). Atoms are designated as shown in Table 5.

Dihedral	C_0	C_1	C_2	C_3	C_4
FnOH					
C_F-C_F-C_F-F	1.4644	1.8828	0	-3.3472	0
C_F-C_F-C_F-C_F	14.91596	-22.56431	-39.41328	11.61479	35.44685
C_F-C_{OH}-O-H_O	0.26778	-9.36798	9.1002	0	0
F-C_F-C_F-F	-4.707	6.799	0	-2.092	0
C_F-C_F-C_{OH}-O	-1.21963	-0.182	-0.50627	0.63596	1.27194
C_F-C_F-C_F-C_{OH}	4.97059	-11.68591	-7.15045	5.79902	8.06675
F-C_F-C_{OH}-H_C	0.60668	1.82004	0	-2.42672	0
F-C_F-C_F-C_{OH}	1.38281	4.14844	0	-5.53125	0
F-C_F-C_{OH}-O	0.9686	2.90579	0	-3.87438	0
C_F-C_F-C_{OH}-H_C	0.37865	1.13596	0	-1.51461	0
H_C-C_{OH}-O-H_O	0.99579	2.98738	0	-3.98316	0
HnOH					
C_H-C_H-C_H-H	0.6276	1.8828	0	-2.5104	0
C_H-C_H-C_H-C_H	0.51879	-0.23019	0.89681	-1.49134	0
C_H-C_{OH}-O-H_O	-0.79464	3.75594	0.06712	-3.12296	0
H-C_H-C_H-H	0.6276	1.8828	0	-2.5104	0
C_H-C_H-C_{OH}-O	2.97554	1.25728	1.11423	-5.33767	0
C_H-C_H-C_H-C_{OH}	0.51879	-0.23019	0.89681	-1.49134	0
H-C_H-C_{OH}-$H_{CH2OH,methylene}$	0.6276	1.8828	0	-2.5104	0
H-C_H-C_H-C_{OH}	0.6276	1.8828	0	-2.5104	0
H-C_H-C_{OH}-O	0.60436	1.6448	-0.13816	-2.23317	0
C_H-C_H-C_{OH}-$H_{CH2OH,methylene}$	0.6276	1.8828	0	-2.5104	0
$H_{CH2OH,methylene}$-C_{OH}-O-H_O	0.76205	2.37159	0.0609	-3.18897	0

Appendix B

Table 9 - Characterisation of the different simulated systems.

Base molecule	Box side length (nm)	Number of water molecules	Number of alcohol molecules	Molecular area (nm^2/molecule)
F18OH	18.2	40000	10	33.1
F18OH	18.2	40000	5	66.2
F18OH	9.1	10000	138	0.6
F18OH	9.1	10000	83	1
F18OH	9.1	10000	64	1.29
F18OH	9.1	10000	39	2.12
F18OH	9.1	10000	21	3.94
F18OH	9.1	10000	13	6.37
F18OH	9.1	10000	10	8.28
F18OH	18.2	40000	550	0.6
F16OH	18.2	40000	550	0.6
F14OH	18.2	40000	550	0.6
F12OH	18.2	40000	550	0.6
H18OH	18.2	40000	550	0.6
H16OH	18.2	40000	550	0.6
H14OH	18.2	40000	550	0.6
H12OH	18.2	40000	550	0.6

Appendix C

Hydrogenated Alcohols GIXD spectra

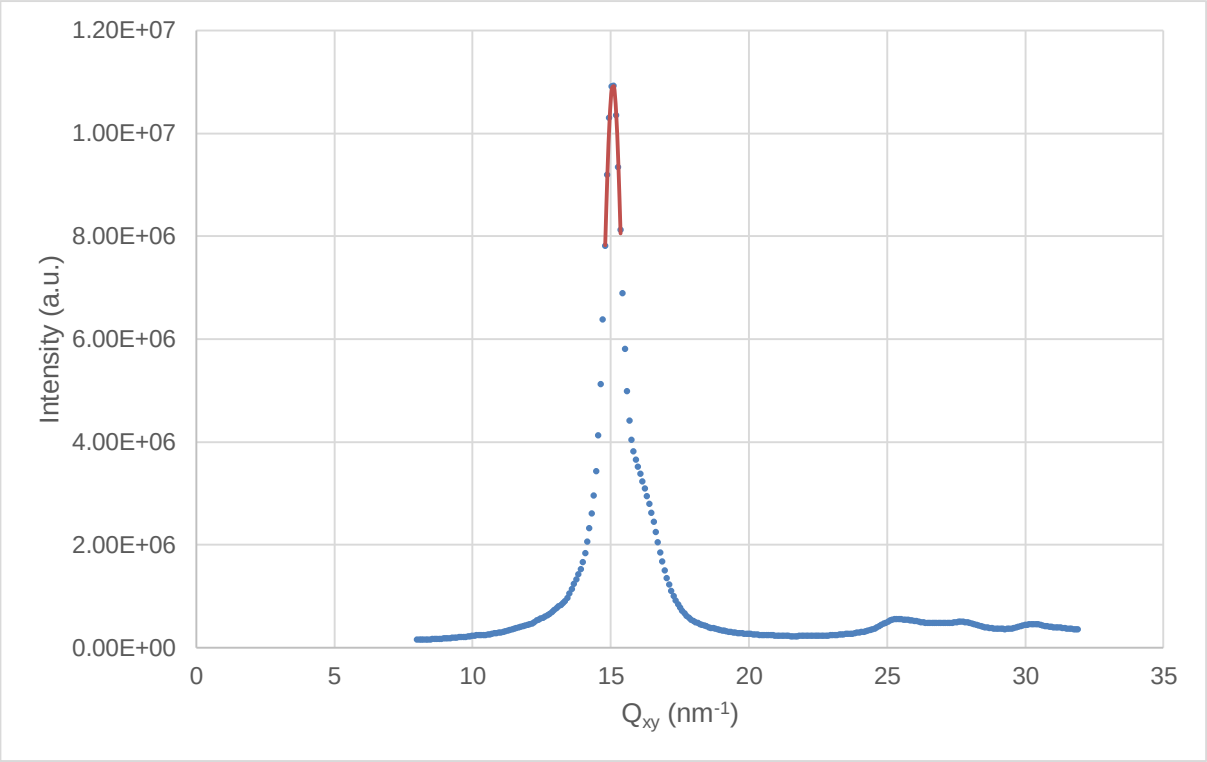

Figure 31 - Simulated diffraction spectra and Gaussian fits for the presented peaks for a system of 550 H18OH molecules at a molecular area of 0.6 nm^2/molecule (18.2 nm side box).

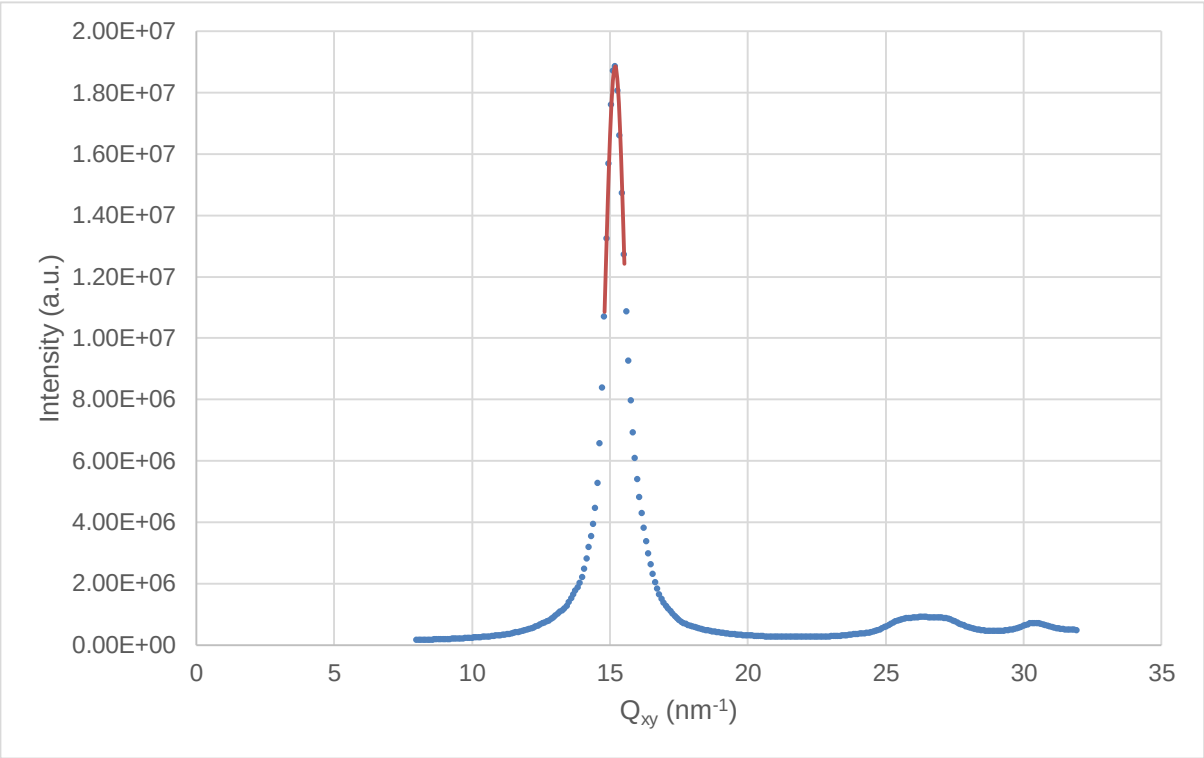

Figure 32 - Simulated diffraction spectra and Gaussian fits for the presented peaks for a system of 550 H16OH molecules at a molecular area of 0.6 nm^2/molecule (18.2 nm side box).

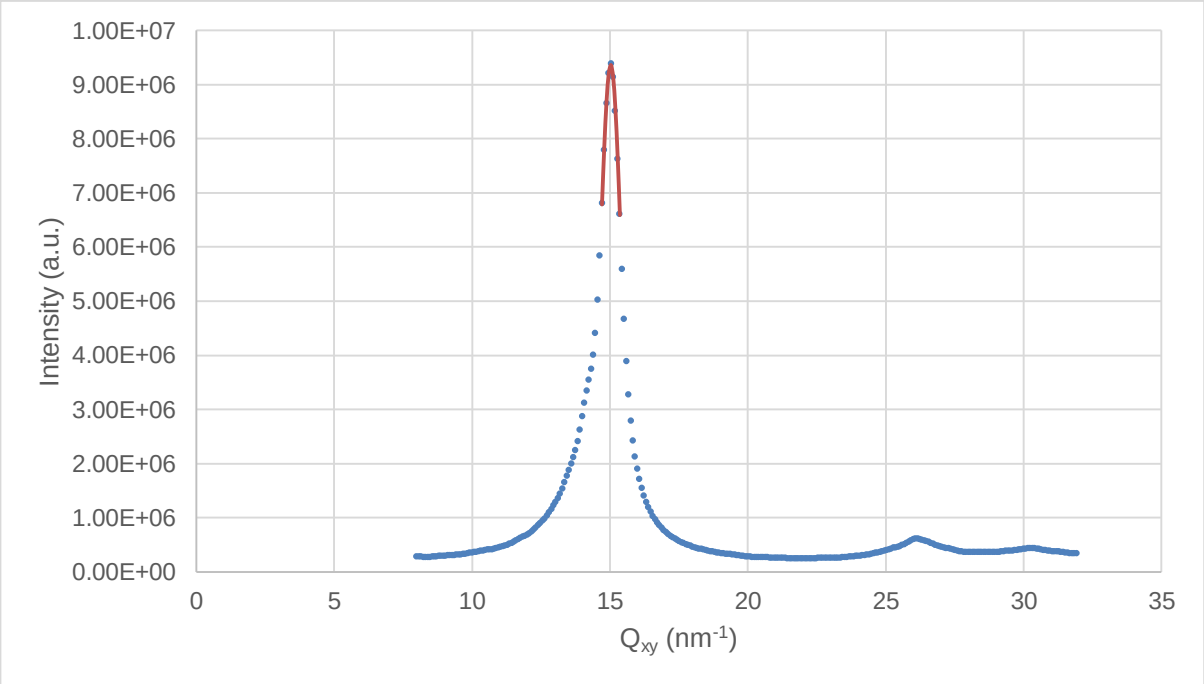

Figure 33 - Simulated diffraction spectra and Gaussian fits for the presented peaks for a system of 550 H14OH molecules at a molecular area of 0.6 nm^2/molecule (18.2 nm side box).

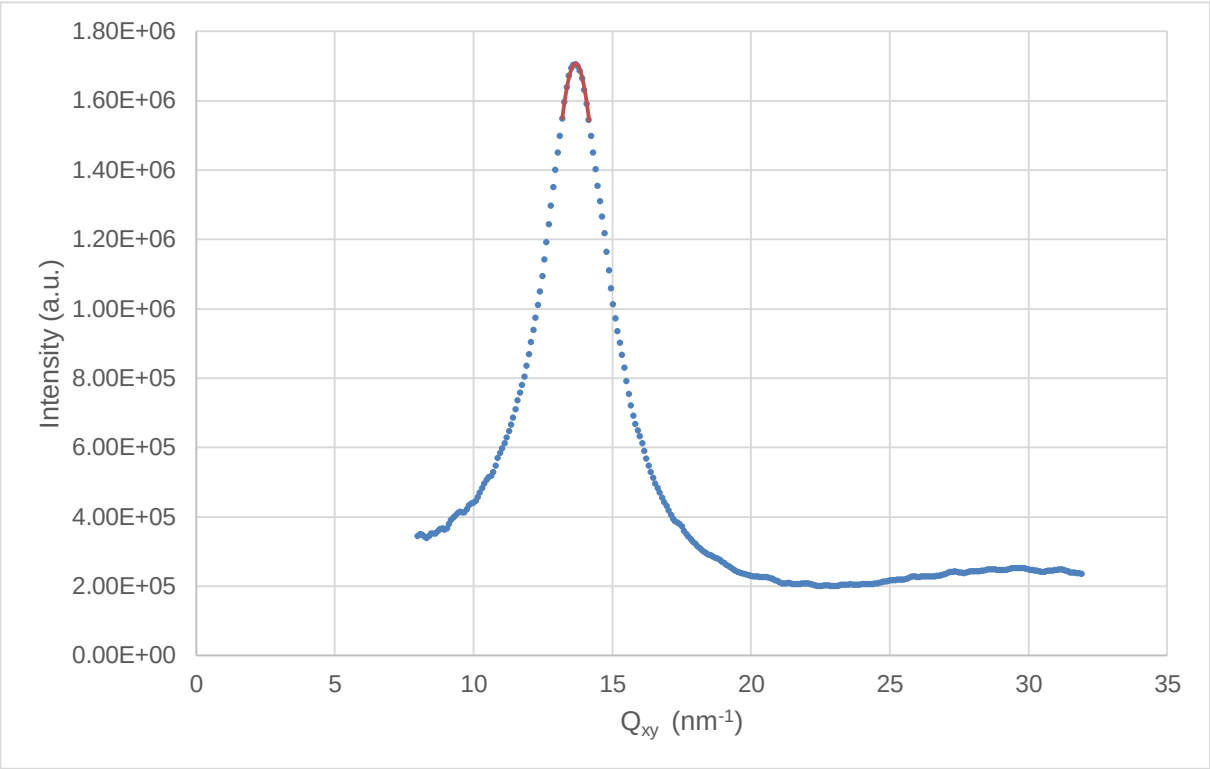

Figure 34 - Simulated diffraction spectra and Gaussian fits for the presented peaks for a system of 550 H12OH molecules at a molecular area of 0.6 nm^2/molecule (18.2 nm side box).